Journal of Building Engineering xxx (xxxx) 104493

Contents lists available at ScienceDirect

Journal of Building Engineering

journal homepage: www.elsevier.com/locate/jobe

Experimental and analytical investigation of drilled flange connections (DFCs) with radial drilling patterns

Peyman Shadman Heidari [a], Armin Aziminejad [b, *], A.S. Moghadam [c], Mohammad Ali Jafari [d]

[a] Department of Civil Engineering, East Tehran Branch, Islamic Azad University, End of Shahid Bahonar Street, 18 km-Shahr Ghiamdasht, Imam Reza Highway, Afsariyeh Highway, Tehran, Iran
[b] Department of Civil Engineering, Science and Research Branch, Islamic Azad University, Daneshgah Blvd, Simon Bulivar Blvd, Tehran, Iran
[c] Department Structural Engineering, International Institute of Earthquake Engineering and Seismology IIEES, No.192 Arghavan St. North Dibaji, Farmaniyeh, Tehran Province, Tehran, Iran
[d] Department of Structural Engineering, Niroo Research Institute, End of Dadman Street, Tehran Province, Tehran, Iran

ARTICLE INFO

Keywords:
Reduced beam section
Drilled flange connection
Hysteretic behavior
Inter-story drift angle
Plastic rotation
Plastic strain

ABSTRACT

The capability of reduced beam sections (RBS) to improve the seismic behavior of rigid connections leads to their notable application in steel moment-resisting frames. However, they may encounter shortcomings such as local buckling and lateral-torsional buckling. To resolve such problems, the idea of utilizing perforated beam flanges instead of cut-out flanges as reduced beam sections was presented. These type of connections can reduce the potential for local and lateral-torsional buckling of conventional RBS connections and improve their seismic performance. Achieving such advantages requires special care to geometrical specifications and drilling patterns (DPs). Appropriate arrangement of holes reduces the stress concentration around the beam flange-to-column Complete Joint Penetration (CJP) groove weld and, consequently, prevents the groove weld and inter-hole area from tearing and fracturing in early cycles of loading. The present study investigated the hysteretic performance of the drilled flange connections (DFCs) of various drilling arrangements through an experimental program.

It should be noted that the box-shaped columns were considered in this study to target the 3D moment resisting frames (MRFs) that all their axes participate in the lateral force-resisting system. The most appropriate drilling patterns were selected using remarkable numbers of numerical analyses. Four laboratory specimens with different drilling arrangements of top and bottom flanges were fabricated based on preliminary numerical analyses. The laboratory specimens were subjected to cyclic loading. To evaluate the specimens' seismic performance, moment-rotation hysteresis curves were compared, and the stress distribution at the connection CJP groove welds. The results of the experimental tests revealed that those DFCs with combined DP with notches and holes (DFC1), radial DP (DFC2), semi radial DP with notches (DFC3), and semi radial DP (DFC4) could increase the rotational capacity of the DFCs up to 50% of the required rotation of the special moment-resisting connections. Moreover, semi radial DP (DFC4) may increase the connection's rotational capacity up to 75% of the special moment-resisting connections. Also, Based on the analytical results, conventional RBS connections may increase the 0.04 radians, needed rotational capacity up to 37.5% for a pre-qualified moment-resisting connection. It was also shown that no lateral-torsional buckling and smaller degradation in stiffness and strength took place in plastic hinge zones at the relative deformation of 0.04 radians. The plastic strain at

* Corresponding author.
E-mail address: Arminaziminejad@srbiau.ac.ir (A. Aziminejad).

https://doi.org/10.1016/j.jobe.2022.104493
Received 5 July 2021; Received in revised form 5 April 2022; Accepted 8 April 2022
2352-7102/

the center of the CJP groove weld line in the beam longitudinal direction was more significant than those corners of the groove weld line in the same direction. In all specimens, the minimum plastic strain of the CJP groove weld took place in central parts of the weld in the transverse direction. In DFC1, DFC2, DFC3, and DFC4 specimens, the contribution of panel zone rotation in the overall plastic rotation of the connection is negligible.

1. Introduction

Welded unreinforced flange (WUF) connections in moment-resisting steel frames' connections suffered a considerable failure during the Northridge earthquake of 1994 in the USA. Such improper performances were attributed to groove welds' inappropriate behavior by several researchers [1–3]. Following the Northridge event, widespread researches were performed to recognize and resolve the problems associated with rigid connections in moment-resisting frames. Some of these researches were presented in SAC reports [4,5]. Those researches were aimed to investigate the reasons for the failure of rigid connections, their failure modes, and the location of damaged zones [6]. Whittaker et al. [7] conducted experimental studies on pre-Northridge connections. They showed that the average plastic rotation of beams in those connections was less than 0.005 radians. After determining the weaknesses of pre-Northridge connections, several studies were conducted to improve their seismic behavior. Getting the inelastic regions away from the critical parts of the connection was one of the proposed techniques. Such a technique led to proposing RBS connections. Kulkarni and Vesmawalab [8] compared the behavior of WUF and RBS beam-to-column connections using numerical analysis and experimental techniques. They revealed that the groove weld fracture in the beam bottom flange-to-column junction leads to the improper behavior of the WUF connection. They also showed that the plastic rotation of the beam in the WUF connection was about 0.02 radians. Engelhardt et al. [9–11] demonstrated that the idea of utilizing RBS connections is a reliable solution for preventing the connection from brittle failure on beam-to-column groove weld. They studied the cyclic behavior of welded flange connections with bolted angles. Their studies on eight full-scale specimens revealed that the connections fractured near the connection groove welds. They also showed that reducing the beam strength at a certain distance from the beam-to-column junction leads to transferring the plastic hinge to the weakened zone. Uang et al. [12] conducted experiments on steel RBS connections with welded haunch. They studied six full-scale specimens and showed that fracture happened at the bottom flange's groove weld. They also showed that the plastic rotation of the connections was less than 0.01 radians. Chen and Chao [13] tested four RBS connections with reinforced concrete (RC) slabs. They examined the effect of composite beam-slab behavior on the performance of the RBS connection. Their studies revealed that the plastic strains distributed in bottom flanges were greater than those in the upper ones. They also demonstrated that the RC slab could increase the RBS connection plastic deformation to 0.045 radians. Jones et al. [14] performed tests on eight full-scale RBS connection specimens with composite slabs. In seven specimens, their inter-story drift angle reached 0.04 radians before exceeding the strength degradation of 80%. They revealed that RBS connections increase energy dissipation without a reduction in connection strength. Roeder [15] demonstrated that since these connections can reach peak plastic rotation of 0.02 radians, they are not suitable from the seismic performance point of view. It should be noted that his conclusions were based on direct cuts on RBS connections. Lee et al. [16] tested eight full-scale RBS connections with bolted and welded shear tabs. They utilized medium-to high-strength panel zones. Based on their studies' results, welded specimens showed the appropriate plastic rotation of 0.04 radians while the bolted ones suffered from brittle failures. In the later specimens, the minimum inter-story drift angle of 0.01 radians was observed in connection panel zones. Chou and Wu [17] proposed a new RBS configuration using reduced flange plates. They fabricated their test specimens based on the results of numerical studies. The results of their numerical and experimental studies can tolerate the plastic rotation of 0.04 radians without considerable strength degradation. The proposed RBS connection was suffered from fracture and local buckling of beam flange. The analytical and experimental studies of Pachoumis et al. [18] on RBS connections emphasized the need for reevaluating the required geometrical specifications of RBS connections. Iannone et al. [19] evaluated the endplate RBS connections and showed that the tested connection could tolerate the plastic rotation of 0.06 radians. Moslehi Tabar and Deylami [20,21] investigated the effect of RBS connections on the column panel zone's ductility and showed the appropriate hysteretic behavior of high-strength panel zones. Their numerical analysis revealed that excessive shear deformation of panel zone and brittle fracture might occur in the connections associated with weak panel zones. They demonstrated that improvement in the seismic behavior of RBS connections is related to the web local buckling and presented new details for postponing the web local buckling. Their proposed connection made about 40% enhancement in the plastic rotation capacity of RBS connections. Kim et al. [22] investigated the seismic behavior of sloped RBS connections with radius cuts. Their experiments showed that the top beam flange-to-column junction's groove weld experienced brittle failure in the plastic rotation of 0.04 radians.

Yang and Popov [23] proposed drilling circular holes in the beam flange to reduce the beam section. They evaluated the different drilling configurations by performing laboratory tests on eight specimens. Based on their study results, perforated beam flanges can prevent the beam from local and lateral-torsional buckling. Still, the stress concentration around holes may cause a premature rupture in such areas. It should be noted, the strain reduction due to perforation was restricted between 2% and 8% of the stiffness of the unperforated section. The results of their studies showed that the plastic rotation capacity of perforated connections was 0.048 radians. Thus, they can meet the required specifications of special steel moment-resisting frames. Farrokhi et al. [24] tested rigid connections with drilled cover plates. They used 30 analytical models as well as three experimental specimens. They considered I shaped built-up columns in analytical models. The section reduction was made by drilling a single row of holes in the flange axis's orthogonal direction. The circular hole diameters were considered to be within the ranges of 6 mm–30 mm and 8 mm–36 mm for top and bottom cover plates. The hole diameters and their spacing were restricted to 0.8 and 1.25 of the cover plate thickness. The experiments

showed that the drilled cover plate prevents the connection from the beam flange-to-column groove weld's failure. The rotational ductility capacity of such connections was calculated to equal eight. Vetr et al. [25,26] conducted laboratory tests to evaluate the seismic performance of two DFC specimens. The beam flanges were directly welded to columns. Two parallel rows of holes with incremental diameters were drilled on beam flanges. The specimens were subjected to cyclic loads. The I-shaped sections were used for columns in both specimens. One of the specimens had a weak panel zone, and the other had a strong one. The test results showed that the rotational capacity of the tested DFCs was 0.05 radians. Local buckling and the fracture of the flange were observed in the inter-hole area. It should be noted that the panel zones were rotated about 0.0057 radians without any failure at the column face. Lee et al. [27] investigated the seismic behavior of bolted end plate DFCs based on experimental studies on four full-scale specimens. They examined four different drilling patterns. Two and four rows of holes of the particular diameters were considered in test specimens. The results revealed that the examined connections were tolerated by the plastic rotations of about 0.04 radians. The beam flange among the holes buckled and ruptured at its ultimate limit state. Atashzaban et al. [28] evaluated the equivalent plastic strain, the triaxial index, and the rupture index of beam flange-to-column junction groove weld in six WUF, one regular RBS, and four DFC connections. Their numerical study showed that one could reduce the rupture index by providing an appropriate drilling arrangement in DFCs. Also, the equivalent plastic strain could reduce about 40% of WUF and conventional RBS connections. They also showed that utilizing strong panel zones can reduce stress concentration in connection groove weld and, consequently, better performance of DFCs. Ahmady [29] evaluated the effect of design parameters such as the hole spacing, the hole diameter, the number of drilling rows, and the span length-to-beam height ratio of DFCs on their seismic performances. To this end, they used numerical analysis validated by the experimental studies presented by Vetr et al. [25,26]. The results of his study revealed that DFCs could reduce the equivalent plastic strain and the rupture index in the CJP welds by about 100% and 154%, respectively. Tahamouli Roudsari et al. [30] investigated the seismic performance of DFCs. They considered two rows of holes besides vertical and diagonal stiffeners installed in the plastic hinge zone. Based on numerical analyses on 15 models and experiments on three specimens, they showed that the mentioned stiffeners could increase the energy dissipation capacity without a noticeable change in ultimate strength. Peyman Shadman Heidari et al. [31] presented new drilled flange connections with combined arrangements of holes and notches. They studied two experimental specimens and 24 numerical models. Among the studied arrangements (i.e., WUF, RBS, DFCs with inclined, parallel, and combined notches and holes drilling patterns), CDFC with combined notches and holes drilling patterns performed better than the other connections, remarkable reductions in damage indexes were observed in connection.

In this study, to overcome the shortcomings of DFCs and improve their cyclic behavior, connections with new DPs were proposed. DFCs with different arrangements of perforation and varying hole diameters were investigated. Such perforating arrangements postpone the rupture and local buckling of beam flange in the reduced section and improve the connection's energy dissipation and rotational capacity. The appropriate drilling arrangements were selected based on the design provisions of RBS connections as well as with different drilling arrangements on the beam flange and finite element (FE) analyses. Various finite element models were prepared to create a proper distribution of plastic strains in the reduced cross-section of the beam flange. In these models starting from investigating linear and uniform drilling arrangements [31], new arrangements with combined holes and notches, radial and semi-radial, were proposed. Four full-scale experimental samples were prepared based on the results of numerical analyses and subjected to cyclic loading. The fabricated specimens were of box type column and drilled flange connection with direct beam flange-to-column welded junctions. Each specimen can be considered as a representative of an appropriate type of connection from the drilling arrangement point of view. The selected drilling patterns were combined DP with notches and holes (DFC1), radial DP (DFC2), semi radial DP with notches (DFC3), and semi radial DP (DFC4) drilling arrangement. Following the application of the loading protocol, the plastic strain distribution around the beam flange-to-column groove weld, the plastic strain in the perforated zone, the deformations of the panel zone, and failure modes were assessed. Finally, the rotational capacity and the energy dissipation of the connections were compared according to the parameters mentioned above.

2. Experimental investigation of DFC with direct beam-to-column connection

2.1. Experimental specimen details

The geometrical specifications of the connection elements (e.g. beam, column, connecting elements, and plates) were calculated based on the hydraulic actuator's capacity, which is 500 kN. It should be noted that structural elements were designed according to ANSI/AISC360-16 [32] and ANSI/AISC341-16 [33]. In order to calculate the distance between the first hole from the column face, ANSI/AISC 358-16 [34] provisions were considered. By increasing the distance from the column flange, the hole diameters were increased linearly. The V_{pz}/V_y (V_{pz} = Shear force at panel zone and V_y = the shear yield force of panel zone) was set to 0.7 according to FEMA355D [35] and FEMA360 [36]. Based on the force capacity of the hydraulic jack, the required flexural strength, and required shear strength for the design of the beam were considered 226.1 kN.m and 147.1 KN, respectively. Also, the required axial, shear and flexural strength for the column were equaled 147.1 KN, 36.6 KN, and 113.1 kN.m, respectively. The shear strength of connection was provided by utilizing the shear tab welded to the column flange consisting of a double plate. Besides, continuity plates were considered in panel zones. The detail of DFCs is illustrated in Fig. 1. Table 1 presents the geometrical specifications of connection elements.

To evaluate the behavior of the DFCs, numerical studies were conducted using multi-purpose ANSYS R16 finite element software. Considering the laboratory's limiting conditions, the results of numerical analyses were evaluated, and the most appropriate DFCs were selected. It should be noted that moving away from the column face, the amount of moment in the beam due to seismic loads decreases. Therefore, to maintain a uniform and widespread distribution of plastic strain in the plastic hinge length, reducing the beam

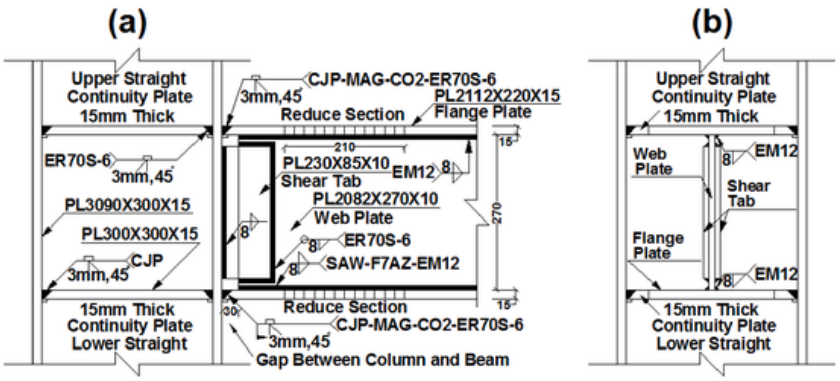

Fig. 1. The fabrication detail of DFC, a) side view, b) front view (Dimensions are in millimeters).

Table 1
Geometrical specification of beam and column and the utilized plates.

Beam flange thickness t_{bf} (mm)	Beam web thickness t_{bw} (mm)	Column flange thicknesst_{cf} (mm)	Column web thickness t_{cw} (mm)	Shear plate thickness t_{st} (mm)	Continuity plate thickness t_{cp} (mm)	End plate thickness t_{ep} (mm)
15	**10**	**15**	**15**	**10**	**15**	**30**

Dimensions are in millimeters.

flange should be increased by increasing the distance from the column face in the flange reduction area. So in the most appropriate DFCs, the drilled hole diameters had a linear increment by getting away from the column face.

Four arrangements of drilling were selected: The combined DP with notches and holes (DFC1), radial DP (DFC2), semi radial DP with notches (DFC3), and semi radial DP (DFC4) drilling arrangement. To assess these drilling patterns in DFCs, four different specimens were fabricated (See Fig. 2). The DP of beam flanges was created in two rows along the flange with five transverse rows. In general the hole diameters were 24 mm, 28 mm, 30 mm, 32 mm, 34 mm, 40 mm, 45 mm, 50 mm and 55 mm which provided 22%, 25%, 27%, 29%, 31%, 36%, 41%, 45% and 50% reduction in the flange cross-sectional area respectively. It is worth mentioning that the drilling patterns were selected to allow widespread inelastic behavior in drilled areas. Hence, the flange reduction was applied in five transversal rows with a linear increment. According to ANSI/AISC358-16 [34] the distance of the first hole from the column flange “a", the plastic hinge length “b", and “c" the depth of cut at center of the reduced beam section with radius cut for the conventional RBS were calculated to satisfy the following limitations:

$$0.5b_{bf} \le a \le 0.75b_{bf} \tag{1}$$

$$0.65d_b \le b \le 0.85d_b \tag{2}$$

$$0.1b_{bf} \le c \le 0.25b_{bf} \tag{3}$$

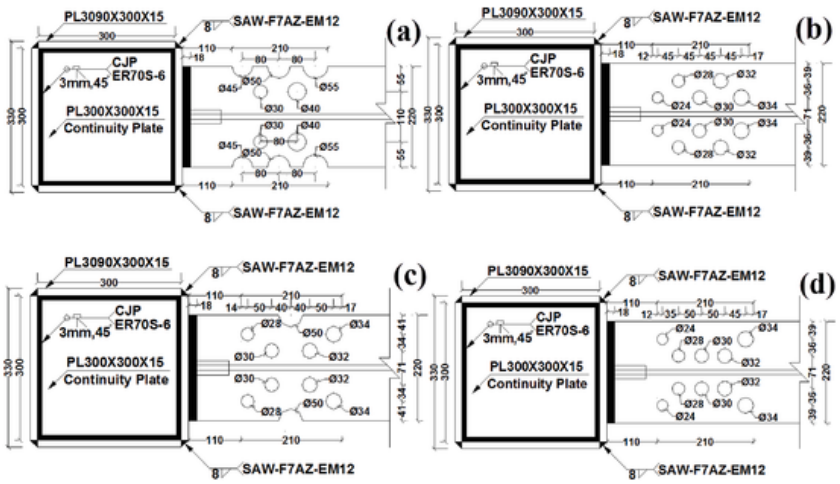

Fig. 2. The drilling details of beam flange in suggested connections, a) DFC1, b) DFC2, c) DFC3, and d) DFC4 (Dimensions are in millimeters).

Where b_{bf} and d_b are beam flange width and depth, respectively, in the first specimen were used a combination of interior and exterior circular holes. Such a configuration produces a sawtooth-shaped section. According to Equation (3), the minimum and maximum reduction of the cross-sectional area of the beam flange with radius cut is 20% and 50%, respectively. The hole diameters of 45 mm, 50 mm, and 55 mm were used to perforate the beam flange edges, making 20%, 23%, and 25% reductions in the flange cross-sectional area, respectively. The internal holes were 30 mm and 40 mm in diameter and made 27% and 36% reduction in the flange's cross-sectional area. The distance of the first hole from the column face was 132.5 mm, and the spacing of drilling rows was 40 mm (See Fig. 2a). The second specimen consists of holes with diameters of 24 mm, 28 mm, 30 mm, 32 mm, and 34 mm such holes were made 22%, 25%, 27%, 29%, and 31% reductions flange cross-sectional area, respectively. The distance of the first hole from the column face was 122 mm, and the spacing of drilling rows was 45 mm (See Fig. 2b). The drilling pattern of the third specimen was a combined notch and semicircular arrangement. The edge drilled holes' diameter was 50 mm, making 23% reductions in the flange cross-sectional area. While the internal holes were 28 mm, 30 mm, 32 mm, and 34 mm in diameter, which made 25%, 27%, 29%, and 31% reduction in the cross-sectional area of beam flange, respectively. The distance of the first hole from the column face was 124 mm, and the spacing of drilling rows was 40 mm and 50 mm (See Fig. 2c). In the fourth specimen, the semicircular drilling pattern was used. The drilled holes were 24 mm, 28 mm, 30 mm, 32 mm, and 34 mm in diameter, which made 22%, 25%, 27%, 29%, and 31% reduction in the cross-sectional area of the flange, respectively. The distance of the first hole from the column face was 122 mm, and the spacing of drilling rows was 35 mm, 50 mm, and 45 mm (See Fig. 2d).

The different arrangements of drilling in the beam flange can be imagined according to the dimensions of the reduced area of the beam flange and the distance of the first hole from the face of the column, based on AISC358-16 [34] steel regulations. The position of the holes and the diameter of the holes in the reduced area of the beam flange must be properly selected, to be able to use the maximum energy absorption capacity of the reduced area of the beam flange in the plastic rotations up to 0.04 radians. The selection of these points for drilling should be such that the strain concentration between the holes is avoided. The concentration of these strains in the limited area can cause premature rupture of the beam flange and failure of this area in small deformations. The research by Peyman Shadman Heidari et al. [31] showed that improper selection of the location of the holes could lead to a decrease in seismic performance and increase equivalent plastic strain and rupture index and cause concentration of stress in the weld line of the beam-column connection. Therefore, the location and diameter of the holes in the beam flange are effective in the seismic performance of the drilled flange connections. The parameters “a" and “b" are the distance of reduced area from the face of the column and the length of the reduced section that considered codes recommended values. The main focus of this study was the appropriate pattern of drilling in the reduced area and the distance recommended by RBS design codes. In this study, the values of “a" and “b" are considered constant for the experimental specimens according to AISC code 358-16 [34]. Therefore, the seismic behavior of the DFCs connection can be investigated with various drilling arrangements of the beam flange in the plastic hinge length. It is also possible to compare the seismic behavior of these types of proposed connections.

2.2. Drilling method

Drilling is a process for making a hole in a metal surface used to make a connection. Drilling can be done in different sizes, with the best quality and the shortest time. There are two methods for creating holes in steel plates with different thicknesses, punching, and drilling. In the punching technique, holes have made by a machine that produces the required shear force for cutting with the help of hydraulic pressure. A punching system increases the speed of perforation, but in terms of quality, punched holes are at a lower level than holes created with rotary drilling. The method of drilling a hole with a column drill is to remove or dig out the metal surface with a drill and pressure. In the column drilling method, the quality of work is excellent. A magnetic drilling machine is a drilling tool in metal with magnetic bases that can drill holes in one step and with great speed and comfort. Its magnetic base makes the device stick to the metal surface and can make drilling easy in any environment. Round drills and spiral drills are tools usually installed on magnetic drilling machines and are used for drilling. The appearance of drills has been very simple in the past, but with the passage of time and the advent of new technologies in the production of drills, the shape of drills has changed, so that today different types of drills are produced in different sizes and shapes. Hot cutting is another common method of cutting plates. In the hot cutting method, a high thickness iron sheet can be cut at high speed. Reduced yield strength, residual stress, and brittleness in a part of the plate can be considered disadvantages of hot cutting.

In this study, the column drill and the round drill method have been used for drilling the beam flanges. The magnetic drilling machines (with round or spiral drill bits) can be a better candidate to create DFC connections due to the extensive advances in industrial tools and suitable equipment in the drilling steel sheets. It is possible to have a suitable speed and accuracy using rotary drilling comparable to the usual lateral cut of beam flange to reduce the beam flange cross-section. Also, it is possible to create a suitable accuracy in reducing the beam flange by drilling, according to the proposed patterns, to achieve the desired behavior. Since the magnetic drilling machine can be attached to steel parts in any situation, it makes it possible to use for drilling steel sheets in any position (such as overhead) and height. Therefore, it is possible to drill the beam flanges at any position and height by connecting magnetic drilling machines to the top or bottom beam flange. Furthermore, due to the upper beam flange location under the roof slab, it is possible to drill the beam flange from under the roof with a magnetic drilling machine to retrofit the connections of steel moment-resisting frames. This method is done by creating minimum thermal problems and residual stresses. Therefore, it is easy and accurate with better safety. Also, in many cases, The steel frame and steel parts are made in the factory. Then a magnetic drilling machine or punching machine can be used to perforate these parts adequately.

The arrangement and pattern of drilling in beam flange have an essential and effective role in preventing the concentration of plastic strains between the holes and preventing premature rupture of these parts. Therefore, the proper performance of this type of connection can be expected by selecting the most suitable beam flange drilling pattern by the operating conditions. Furthermore, it is

possible to retrofit and protect the CJP groove welds of the beam flange to column connection from premature rupture with lower cost due to the modern tools available for drilling the beam flange.

2.3. Test setup

Four full-scale test specimens were fabricated and subjected to quasi-static loading protocols. It is worth mentioning that the same box-shaped columns were considered for all specimens. The tests were performed in the Structural Engineering laboratory of the International Institute of Earthquake Engineering and Seismology (IIEES). Figs. 3 and 4 illustrate the test setup and the specifications of specimens, respectively.

Considering the capacity and dimensions of the reaction frame, the column height and the beam length were set to 3090 mm and 2112 mm, respectively. Furthermore, the distance of the loading point on the beam was 1537 mm from the column face.

Pinned connections were considered as column supports. Furthermore, lateral supports were utilized to prevent the beam from total lateral-torsional buckling. Fig. 5 indicates a view of a test specimen, a hydraulic actuator, and column supports.

2.4. Material properties

The steel plates of the ST-37 type were used to fabricate beams, columns, and plates. To accurately measure the mechanical properties of steel elements, tensile tests were conducted on steel samples according to ASTM-A370-14 [37]. For every full-scale specimen, a coupon was prepared for 10 mm and 15 mm plates. Figs. 6 and 7 present a view of test coupons and their stress-strain curves, respectively. In shear tabs, column endplates, and web-to-flange junctions in columns and beams, fillet welds were used. The submerged-arc welding technique was used to mount the steel elements of beams and columns. Based on the AWS A5.17 standard, a 4 mm magnesium electrode of type EM12 was used along with F7AZ (KJF-510) flux. Fully penetrated groove welds were used for

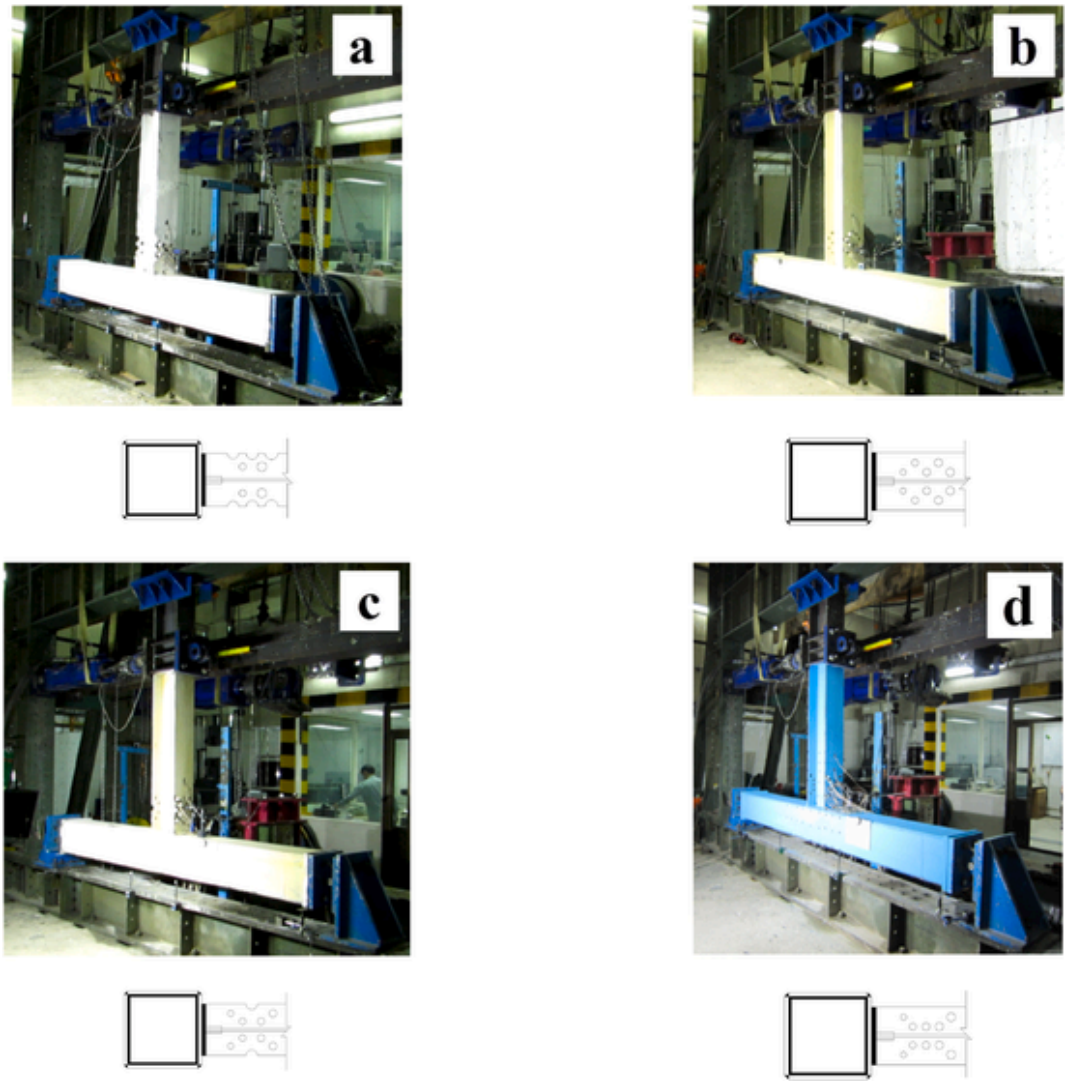

Fig. 3. A general view of test setup and drilling patterns for a) DFC1, b) DFC2, c) DFC3, and d) DFC4.

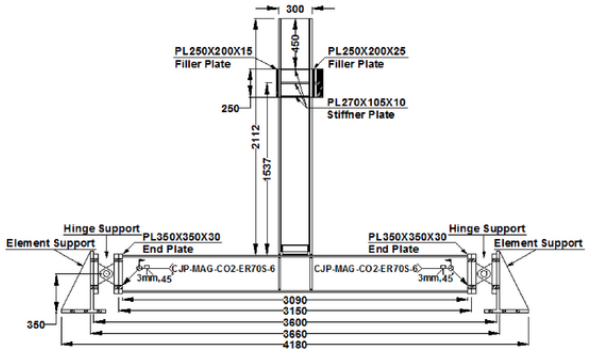

Fig. 4. A view and general dimensions of specimens (units in mm).

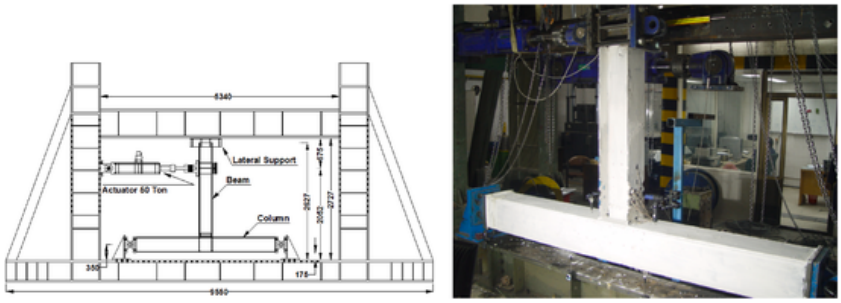

Fig. 5. A view of a specimen DFC1 in reaction frame (units in mm).

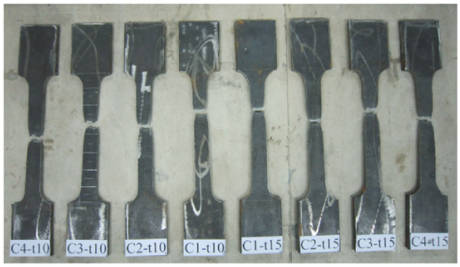

Fig. 6. Tensile test samples.

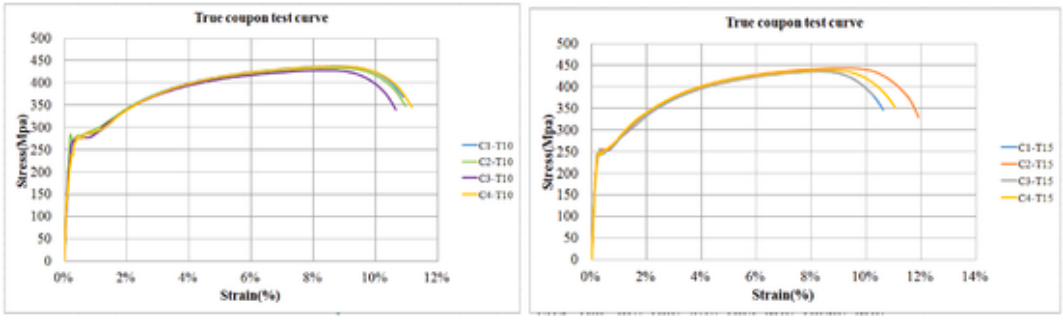

Fig. 7. The stress-strain curve of test coupon with a thickness of 10 mm and 15 mm.

beam flange-to-column junctions and mounting continuity plates. The gas metal arc welding (GMAW) technique was used to connect beam flanges to columns.

Furthermore, column caps, shear connections, and continuity plates were mounted by the GMAW technique. For the welding, CO_2 gas was used as a weld protector, and 1.2 mm ER70S-6 electrodes were used according to AWS A5.18. The mechanical specifications of steel elements and electrodes are tabulated in Table 2.

To calculate the beam's nominal flexural strength (M_p) with I shape cross-sectional according to the results, Equation (4) was used.

Table 2
Engineering mechanical properties of utilized materials.

Specimen	Coupon test	Beam web		Column web		Beam web		Column web		Weld (EM12,4 mm)		Weld (ER70S-6,1.2 mm)	
		F_y (Mpa)	F_u (Mpa)	F_y (Mpa)	F_u (Mpa)	ε_y (%)	ε_u (%)	ε_y (%)	ε_u (%)	F_y (Mpa)	F_u (Mpa)	F_y (Mpa)	F_u (Mpa)
DFC1	C1-t15	-	-	244.2	402.8	-	-	0.39	10.6	411.9	505	421.7	573.7
	C1-t10	282	403.3	-	-	0.66	10.9	-	-				
DFC2	C2-t15	-	-	253.8	406.3	-	-	0.45	11.9				
	C2-t10	281.2	399.8	-	-	0.53	10.9	-	-				
DFC3	C3-t15	-	-	248.2	401.7	-	-	0.35	10.3				
	C3-t10	276.1	395.8	-	-	0.62	10.6	-	-				
DFC4	C4-t15	-	-	246.5	403.7	-	-	0.37	11				
	C4-t10	275.2	402.2	-	-	0.51	11.2	-	-				

Unit: N and mm.

$$M_p = b_{bf} t_{bf} (t_{bf} + h_{bw}) F_{ybf} + 0.25 t_{bw} h_{bw}{}^2 F_{ybw} \tag{4}$$

In this equation b_{bf} t_{bf} t_{bw}, and h_{bw} are the flange width, the flange thickness, the web thickness, and the web depth of the beam, respectively. Also, F_{ybf} and F_{ybw} are specified minimum flange yield stress and specified minimum web yield stress of the beam, respectively. Therefore, according to Equation (4) and Tables 1 and 2, the beam's nominal flexural strength values for the proposed connections DFC1, DFC2, DFC3, and DFC4 will equal 281.0 289.9, 283.7, and 282.0 kN.m, respectively.

2.5. Test procedure and cyclic loading

Hysteresis curves are required to evaluate the seismic behavior of moment resisting connections and investigate their ductility, strength, and stiffness. Hence, in this study, cyclic loading was considered. A 500 kN hydraulic actuator with the ultimate stroke of ±150 mm was used to apply cyclic loads on test specimens. According to ANSI/AISC341-16 [33] cyclic loading protocol, the cyclic loads were applied to the beam outset. Fig. 8 illustrates the loading protocol in which the vertical axis is the relative deformation of the beam outset, and the horizontal axis denotes the loading steps. Accordingly, three stages were considered. Each stage had six constant loading steps. The drift angles of the first three steps were 0.00375, 0.005, and 0.0075 radians which are equivalent to 6.38 mm, 8.51 mm, and 12.77 mm vertical displacements of the beam outset, respectively. The loading steps, as mentioned earlier, were considered to assess the potential for brittle failure in elastic behavior cycles. The drift angles of the fourth and fifth steps were 0.01 and 0.015 radians, equivalent to 17.02 mm and 25.53 mm in deformation of the beam outset, respectively. The increment of 1% was considered in the next loading steps. It should be noted that the maximum drift angle was set to 0.07 radians (equivalent to 119.14 mm vertical displacement of beam end) because of the limitation in the stroke of the actuator.

2.6. Strain and deformation measurement and instrumentation of the specimens

Uniaxial FLA-5-11, biaxial FCA-6 strain gauges, and triaxial FRA-6 rosettes were used to measure inelastic strains. Linear variable differential transformers (LVDTs) were used to measure the deformation of panel zones and beam end displacements as well as the probable displacements of supports and local buckling in the plastic hinge zone. In the examined specimens, the corner and middle parts of the beam-to-column groove weld, the inter-hole area of the plastic hinge zone, the central parts of the beam flange, the corner and central areas of panel zones, and the column flange surfaces above the beam junction were the critical areas of the connection. In order to evaluate the variation in inelastic strain in the middle and corners of the welding lines, the inter-hole areas of plastic hinge zones, and the corner of panel zones, FCA-6 biaxial strain gauges were utilized. Uniaxial strain gauges were used for measuring the strains in the middle of the beam flange. FRA-6 rosettes were used to measure the inelastic strains at the center of panel zones. The arrangements of strain gauges are presented in Figs. 9 and 10.

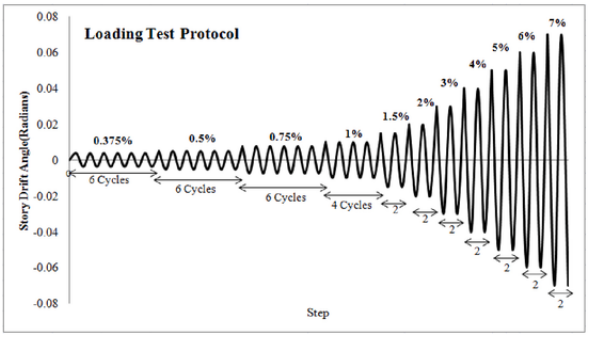

Fig. 8. The considered loading protocol according to ANSI/AISC341-16 [33].

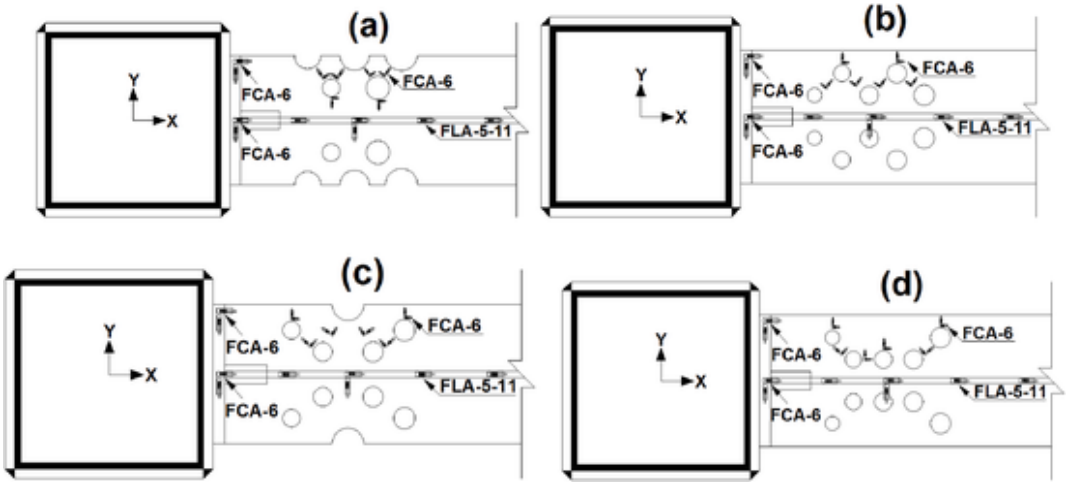

Fig. 9. The arrangement of FLA-5-11 and FCA-6 strain gauges on beam-to-column connection groove weld and beam flange of a) DFC1, b) DFC2, c) DFC3, and d) DFC4.

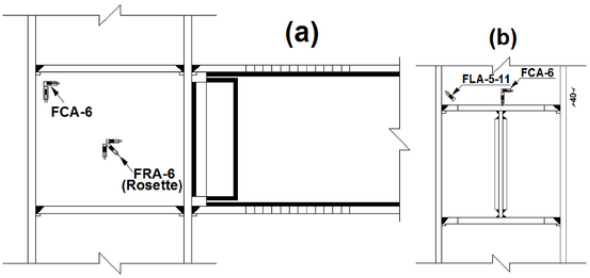

Fig. 10. The arrangement of FLA-5-11, FCA-6, and FRA-6 strain gauges on a) panel zone b) column flange (units in mm).

LVDTs were utilized to measure the shear deformation of the panel zones, deformation of the plastic hinge due to local buckling, and the probable displacements of supports. Hence, as illustrated in Fig. 11, LVDTs were placed at the locations mentioned earlier.

The rotation of the panel zone can be calculated using the following Eq.:

$$\theta_{pz} = \frac{\sqrt{a^2 + b^2}}{2ab}(\Delta_1 + \Delta_2) \tag{5}$$

where a and b are the horizontal and vertical dimensions of the panel zone. Also, Δ_1 and Δ_2 are the values of the diagonal deformations measured by the LVDTs.

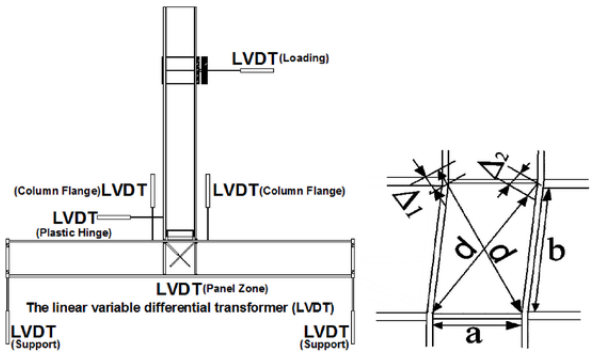

Fig. 11. The arrangement of LVDTs and parameters of panel zone.

3. Experimental results

3.1. The hysteretic behavior of DFC specimens

According to ANSI/AISC341-16 [33], the steel special moment-resisting connections should tolerate the plastic rotation of 0.04 radians. Furthermore, the flexural strength of the connection at the mentioned rotation should not be less than 80% of the beam's plastic bending moment. The hysteresis curves of the examined DFCs are presented in Figs. 12–15. The tests results showed that DFC1, DFC2, and DFC3 could tolerate the plastic rotation of 0.06 radians, and the plastic rotation in DFC4 reached 0.07 radians. The hysteretic behavior of DFC1, DFC2, and DFC3 showed that their bending capacity is greater than 80% of the plastic bending moment of the unreduced beam. Moreover, these connections can increase the drift angles to 1.5 times that of the special moment resisting frames with conventional connections. On the other hand, DFC4 can increase the drift angles to 1.75 times that of the special moment resisting frames with ANSI/AISC358-16 [34] provided connections.

The first specimen's hysteretic behavior revealed that the measured moment corresponding to the connection plastic rotation of 0.04 radians is 364.8 kN.m, which is 1.3 times the plastic bending moment of the unreduced beam. Furthermore, flange local buckling occurred at the inter-story drift angle of 0.06 radians. The bending moment corresponding to such a plastic rotation was 363.8 kN.m. The strength degradation corresponding to the plastic rotation of 0.06 radians was 0.3% of that corresponding to the plastic rotation of 0.04 radians. It is worth mentioning that the ultimate beam strength degradation was 7.7% (See Fig. 12-a). Fig. 12 b indicates the plastic hinge's deformed shape in the drilled area at the inter-story drift angle of 0.04 radians without any evidence of local buckling.

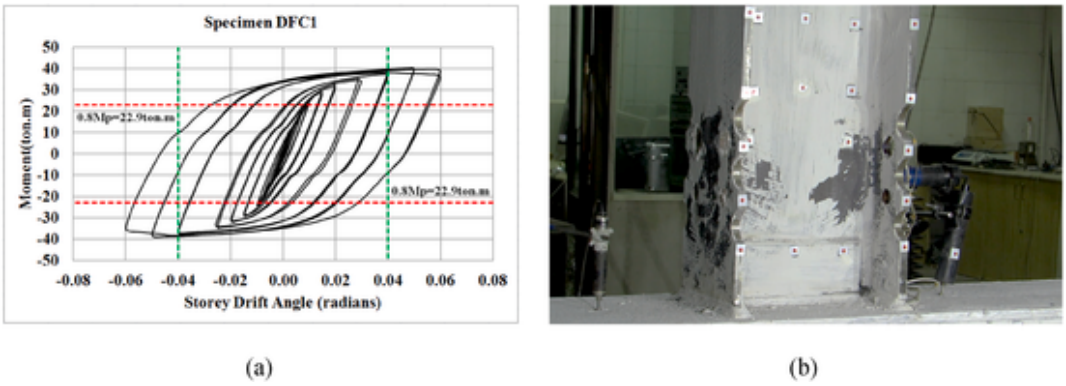

Fig. 12. a) The hysteresis curve of DFC1, b) the deformed shape of DFC1 at the inter-story drift angle of 0.04 radians.

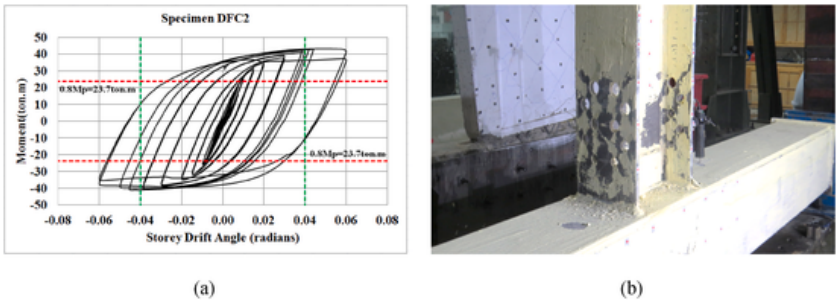

Fig. 13. a) The hysteresis curve of DFC2, b) the deformed shape of DFC2 at the inter-story drift angle of 0.04 radians.

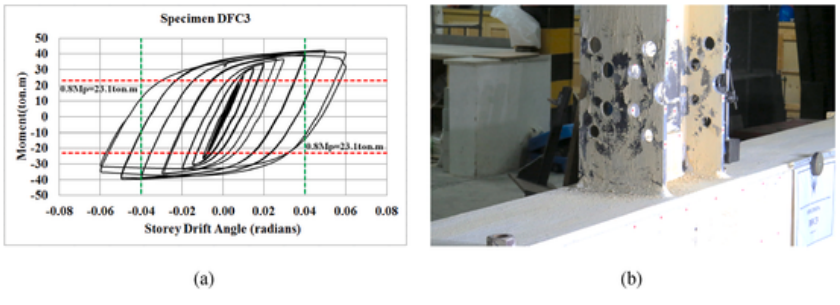

Fig. 14. a) The hysteresis curve of DFC3, b) the deformed shape of DFC3 at the inter-story drift angle of 0.04 radians.

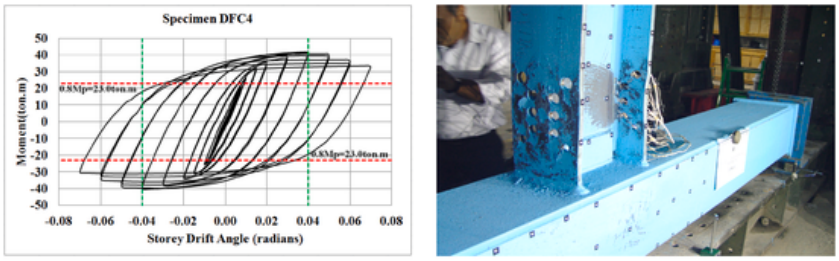

Fig. 15. a) The hysteresis curve of DFC4, b) the deformed shape of DFC4 at the inter-story drift angle of 0.04 radians.

As indicated in Fig. 13-a, in the second specimen, the measured moment corresponding to the connection plastic rotation of 0.04 radians was 404.0 kN.m, which is 1.39 times the plastic bending moment of the unreduced beam. The flange local buckling took place at the inter-story drift angle of 0.06 radians. The bending moment corresponding to such plastic rotation was 365.8 kN.m, greater than 80% of the plastic bending moment. The strength degradation corresponding to such plastic rotation was 9.5% of the plastic rotation of 0.04 radians. It is worth mentioning that the ultimate beam strength degradation was 13.7%. The deformed shape of the plastic hinge in the drilled area at the plastic rotation of 0.04 radians is indicated in Fig. 13-b without any evidence of local buckling in the plastic hinge length.

Fig. 14-a indicates the hysteresis curves of the third specimen. As indicated in Fig. 14-a, the measured moment corresponding to the connection plastic rotation of 0.04 radians was 388.3 kN.m, which is 1.37 times the plastic bending moment of the unreduced beam. Furthermore, local flange buckling occurred at the inter-story drift angle of 0.06 radians. The bending moment corresponding to such plastic rotation was 322.6 kN.m, greater than 80% of the unreduced beam's plastic bending moment. The strength degradation corresponding to the plastic rotation of 0.06 radians was 16.9% of that corresponding to the plastic rotation of 0.04 radians. It is worth mentioning that the ultimate beam strength degradation was 21.5%. The deformed shape of the plastic hinge in the drilled area at the plastic rotation of 0.04 radians is indicated in Fig. 14-b without any evidence of local buckling in the plastic hinge length. The flange local buckling occurred at the inter-story drift angle of 0.06 radians.

The moment-rotation hysteresis curve of the fourth element is indicated in Fig. 15-a. The measured moment corresponding to the connection plastic rotation of 0.04 radians was 409.9 kN.m, which is 1.45 times the plastic bending moment of the unreduced beam. Furthermore, the local flange buckling was observed at the inter-story drift angle of 0.07 radians. The bending moment corresponding to such plastic rotation was 329.5 kN.m, greater than 80% of the plastic bending moment of the unreduced beam. The strength degradation corresponding to the plastic rotation of 0.07 radians was 19.6% of that corresponding to the plastic rotation of 0.04 radians. It is worth mentioning that the ultimate beam strength degradation was 19.6%. The deformed shape of the plastic hinge in the drilled area at the inter-story drift angle of 0.04 radians is indicated in Fig. 15-b without any evidence of local buckling in the plastic hinge length.

The moment-rotation backbone curves of the tested specimens are indicated in Figs. 16 and 17. As indicated in Figs. 16 and 17, almost all the specimens have the same strengths. The maximum strengths were considered in DFC2, while the minimum strength degradation occurred in DFC1. The maximum drift angle capacity was observed in DFC4.

Furthermore, in all the suggested connections perforated beam flange, the bending moment corresponding to the plastic rotation of 0.04 was greater than 80% of the unreduced section's plastic bending moment. Thus, all the specimens met the seismic regulations of ANSI/AISC341-16 [33] for special moment-resisting connections. Moreover, the performances of the examined specimens were better than drilled connections with parallel drilling patterns presented by Vetr et al. [25,26].

The maximum plastic rotation of all DFC specimens was greater than 0.06 radians, which is satisfactory compared to traditional WUF and RBS connections' rotational capacity. Table 3 presents the maximum drift angle capacity, θ_{pmax}, the plastic bending moment of the beam section, M_P, the bending moment corresponding to the plastic rotation of 0.04 radians, $M_{0.04}$, the ultimate flexural strength of the beam, M_{umax}, the minimum plastic bending moment of beam following the local buckling of the flange, M_{umin} and the maximum strength degradation of the beam. As tabulated in Table 3, the minimum and the maximum strength degradation were observed in DFC1 and DFC3.

Table 4 presented the yield rotation, θ_y, the yield bending moment of the beam, M_y, the initial stiffness, $K_{initial}$, and the energy dissipation, E_D, in experimental specimens. As tabulated in Table 4, the maximum and minimum initial stiffness were observed in DFC3 and DFC2, respectively. Furthermore, the maximum energy dissipation belongs to DFC4. Table 5 summarizes the experimental specimens' drift angle capacities and failure modes.

The arrangement and pattern of the drilling beam flange have an important and effective role in preventing the concentration of plastic strains between the holes and preventing premature rupture of these parts. The premature cracks in the CJP groove welds and rupture in the distance between the holes in the reduced area are the critical failure modes in DFCs connections. These critical crack patterns and ruptures could yield uncontrollable failures. The change of the location and arrangement of the holes pattern significantly affects the deformation capacity and the place of rupture in the flange and web of the beam section, So the improper location, arrangement, and diameter of holes in the beam flange will adversely affect the seismic performance and the deformation capacity of the DFCs. Moreover, the stress concentration in the CJP groove welds and between the holes due to improper drilling patterns will

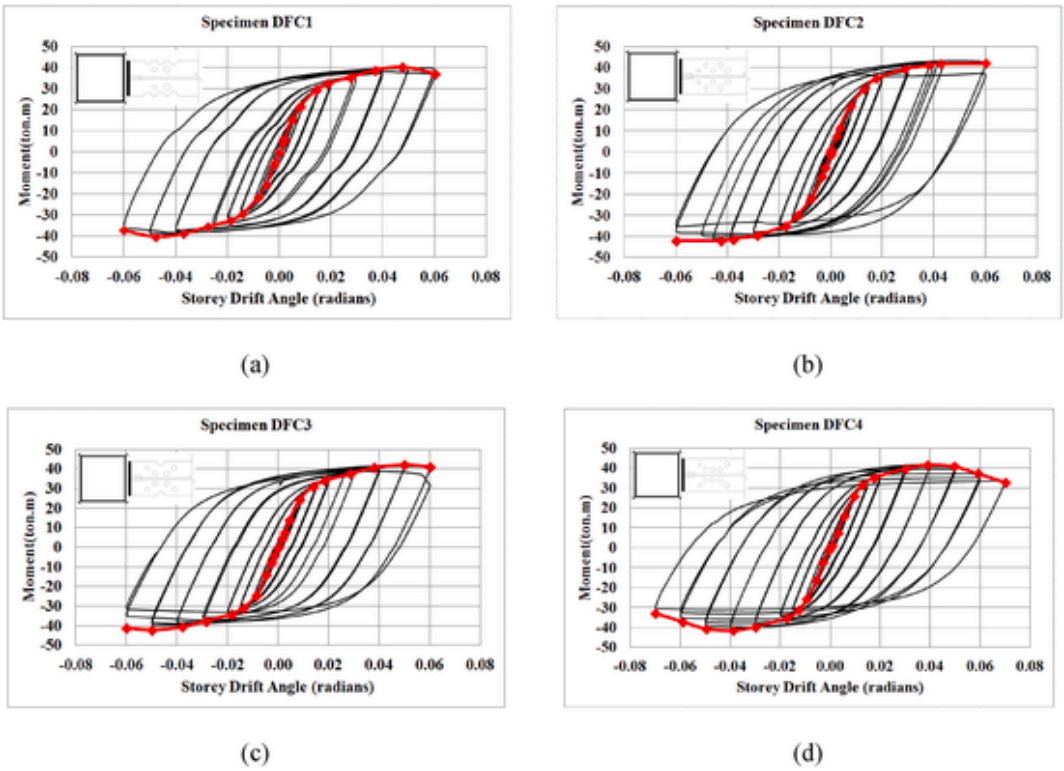

Fig. 16. a) The backbone curves of the hysteresis curves of DFC1, DFC2, DFC3, and DFC4.

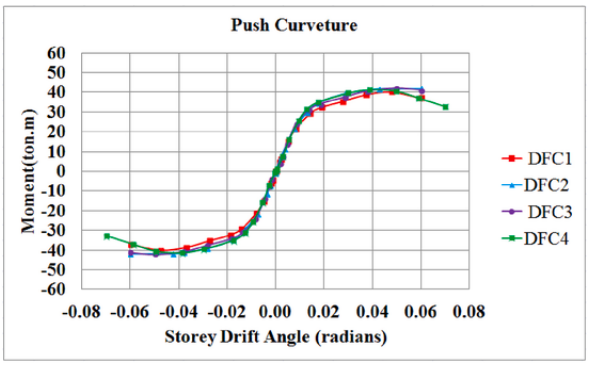

Fig. 17. The comparison of the backbone curves of the hysteresis curves of DFC1, DFC2, DFC3, and DFC4.

Table 3
The summary of experimental data corresponding to bending capacity.

Specimen	θ_{pmax} (radian)	M_p (KN.m)	$0.8M_p$ (KN.m)	$M_{0.04}$ (KN.m)	M_{umax} (KN.m)	M_{umin} (KN.m)	Maximum strength degradation of beam (%)
DFC1	0.06	281.0	224.8	364.8	394.2	363.8	7.7
DFC2	0.06	289.9	231.9	404.0	423.6	365.8	13.7
DFC3	0.06	283.7	227.0	388.3	410.9	322.6	21.5
DFC4	0.07	282.0	225.6	409.9	409.9	329.5	19.6

Unit: KN and mm.

lead to premature rupture at the plastic hinge zone or the CJP groove welds. To avoid these problems, adequate and careful material removal should be achieved.

Using the proposed drilling pattern (DFC4), the rupture between the holes occurred in higher cycles and larger deformations compared to other patterns(DFC1, DFC2, and DFC3). The rotational capacity of the DFC4 increased by up to 25% compared to other proposed drilled flange connections. Also, in the DFC4, no rupture in the flange and web of the beam section occurred at the plastic hinge

Table 4
The initial stiffness and dissipated energy of specimens.

Specimen	θ_y (radian)	M_y (KN.m)	Initial Stiffness $K_{initial}$ (KN/m)	Absorbed Energy E_D (KN.m)
DFC1	0.00812	210.8	25964	315.2
DFC2	0.00756	213.8	28277	347.2
DFC3	0.00852	238.3	27968	364.0
DFC4	0.00936	251.0	26820	422.3

Unit: KN and mm.

Table 5
Summary of drift angle capacities and failure modes.

Specimen	Drift angle capacity (radian)		Controlling failure mode
	Total	Plastic	
DFC1	0.06	0.05188	Rupture of beam flange around drilled areas with 252 mm distance to the column face
DFC2	0.06	0.05244	Rupture of beam flange around drilled areas with 212 mm distance to the column face
DFC3	0.06	0.05148	Rupture of beam flange around drilled areas with 173 mm distance to the column face
DFC4	0.07	0.06064	Without rupture in beam flange

zones compared to other proposed connections at the inter-story drift angle up to 0.07 radians. In DFC1, DFC2, and DFC3, connections rupture occurred in the flange and web of the beam section at the inter-story drift angle of 0.06 radians (See Table 5). Therefore, the change of the location and arrangement of the hole in the beam flanges significantly affects the deformation capacity and the place of rupture in the flange and web of the beam section and could protect the CJP groove welds of the beam flange to column connection from premature rupture.

3.2. Evaluation of the strain of the beam-to-flange connection groove weld

In DFC specimens, the strain gauges were placed on the center and the corners of the beam-to-column groove welds, and the strain values were measured during the cyclic loading. Fig. 18 indicates the strain values of the center and corners of the groove weld in terms of rotation. In all specimens, the strains in the longitudinal direction of the beam (X-direction) were more significant than that of the groove weld line Y-direction. In the X-direction, the measured strain of central areas was more significant than corner strains. While, in the Y-direction, the corner strains were more significant than those measured in the central parts of the groove weld line. A minimum strain in all specimens was in the Y-direction at the central parts of the groove weld line.

The peak value of the X component of strain in the center of the weld line was 3708 μm/m, which was measured in.

DFC3. The X component's minimum measured value in the center of the weld line belonged to DFC2 and was equal to 1893 μm/m. The maximum and minimum Y strain components in the weld center were 912 μm/m and 450 μm/m belonging to DFC2 and DFC1. In the groove weld corner areas, the maximum X component of the strain equal to 2690 μm/m was measured in DFC4. The minimum strain was measured in DFC3 equal to 1320 μm/m. The maximum and minimum measured Y strain components in the weld corner were 1300 μm/m and 700 μm/m belonging to DFC2 and DFC3, respectively. The values of groove weld strains at the inter-story drift angle of 0.06 rad are tabulated in Table 6.

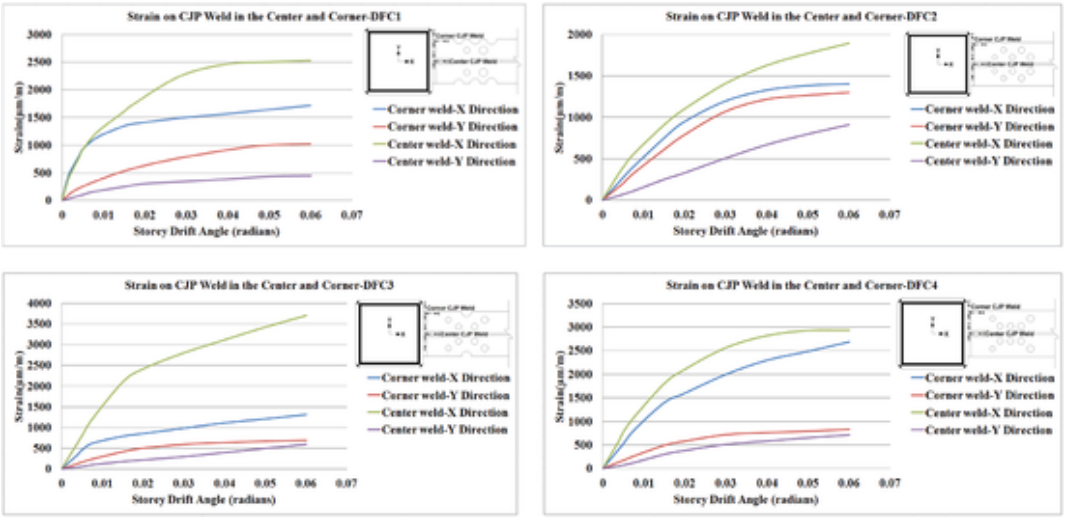

Fig. 18. The strain-rotation curves of the central parts and the corners of groove welds of different DFCs.

Table 6
Groove weld strains at the inter-story drift angle of 0.06 radian (μm/m).

Specimen	Weld line center		Weld line corner	
	X component	Y component	X component	Y component
DFC1	2532	450	1720	1025
DFC2	1893	912	1406	1300
DFC3	3708	600	1320	700
DFC4	2928	710	2690	830

It was shown that the strain values depend on the drilling pattern, their location, and their geometrical specifications. DFC2 and DFC3 drilling patterns are appropriate to reduce the strain values of the center of the CJP weld lines in the X and Y directions, respectively. On the other hand, by utilizing the DFC3 perforating arrangement, one can reduce the strain values in the corner of the weld line in both directions.

3.3. Evaluation of the flange strains in the plastic hinge zone

In a perforation pattern, larger critical path lengths and extended effective areas can be achieved in the drilled zones. The more extensive critical paths can provide a wider plasticized area on the protected area of the flange. Thus, better energy absorption, appropriate plastic strain distribution, and reduced plastic strain of connection groove welds can be achieved. Diagonal paths between holes can delay the local buckling of the drilled zone. Consequently, the extreme flange axial capacity and the maximum potential for plastic hinge ductility can be achieved in such connections. Incremental drilling diameter from the column face leads to the uniform distribution of plastic strain and can increase the connection ductility. To better understand the behavior of selected DFCs, numerical analyses were carried out using ANSYS R16 finite element software [38]. The solid185 element was used in the analytical models. In all numerical models, the mesh size on the CJP groove weld lines was considered equal to 18 × 18 mm (Elkady and Lignos [39]). An RBS connection was designed and modeled to compare the behavior of the proposed perforated beam flange connection with a conventional RBS connection. In this connection, the values of the horizontal distance from the face of column flange to start of RBS cut “a", length of RBS cut “b", and depth of cut at the center of reduced beam section “c" were considered 110, 210 and 33 mm, respectively. The maximum amount of cross-section reduction was considered 30%. The minimum plastic section modulus of the beam section is 840.6 cm^3 in the plastic hinge. The bending capacity of the proposed drilled flange connections with conventional RBS connection has an error of less than 2.4% considering the constant value of material strength, so it will be comparable. Fig. 19 illustrates the distribution of the total strain of beam at the inter-story drift angle of 0.06 radians in proposed DFCs and 0.055 radians (failure rotation) in the RBS connection. As can be seen, using the proposed drilling pattern in beam flange, the plastic strains formed at the plastic hinge zone, and the rupture of the CJP groove welds was prevented for plastic rotations up to 0.06 radians.

To have reliable responses from numerical models, the results of the analytical samples must be in good agreement with the results of the experimental specimens. To validate the FE models, the results of numerical and experimental studies were compared (Fig. 20). As indicated in Fig. 20, there is an acceptable agreement between the results of numerical and experimental studies.

As a result, the strength of DFC connections with appropriate arrangements of holes is increased in comparison with the conventional RBS connection. As shown in Fig. 21, the value of plastic rotation in the combined samples DFC1, DFC2, and DFC3 is 0.06 radians, which is 9.1% higher than the RBS connection. The value of plastic rotation in the sample DFC4 is 0.07 radians, which is 27.3% higher than the RBS connection. DFCs also reduce the potential for local and lateral-torsional buckling of conventional RBS connections. According to the analytical results, The first lateral-torsional buckling in the beam flange for the proposed DFCs and conventional RBS connection occurred at 0.055 and 0.045 radians, respectively. The maximum moment capacity of samples demonstrated in Fig. 21, the maximum moment capacity of the analytical samples DFC1, DFC2, DFC3, DFC4, and RBS is 394.2 kN.m, 396.2 kN.m, 380.5 kN.m, 397.2 kN.m, 348.7 kN.m respectively, which is 13.0%, 13.6%, 9.1%, and 13.9% higher than the RBS sample. Using the proposed DFCs connections could increase the effective cross-section area and the length of critical paths between the holes in the

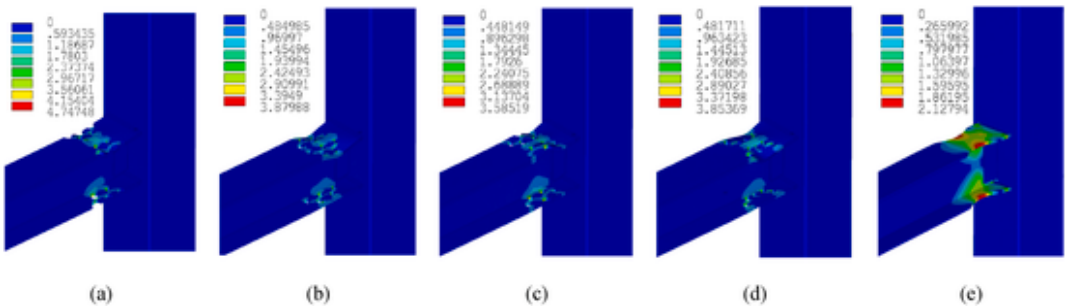

Fig. 19. Distribution of the strain in the plastic hinge zone of samples in the inter-story drift angle of 0.06 radians for DFCs and 0.055 radians for RBS a) DFC1, b) DFC2, c) DFC3, d) DFC4 and e) RBS.

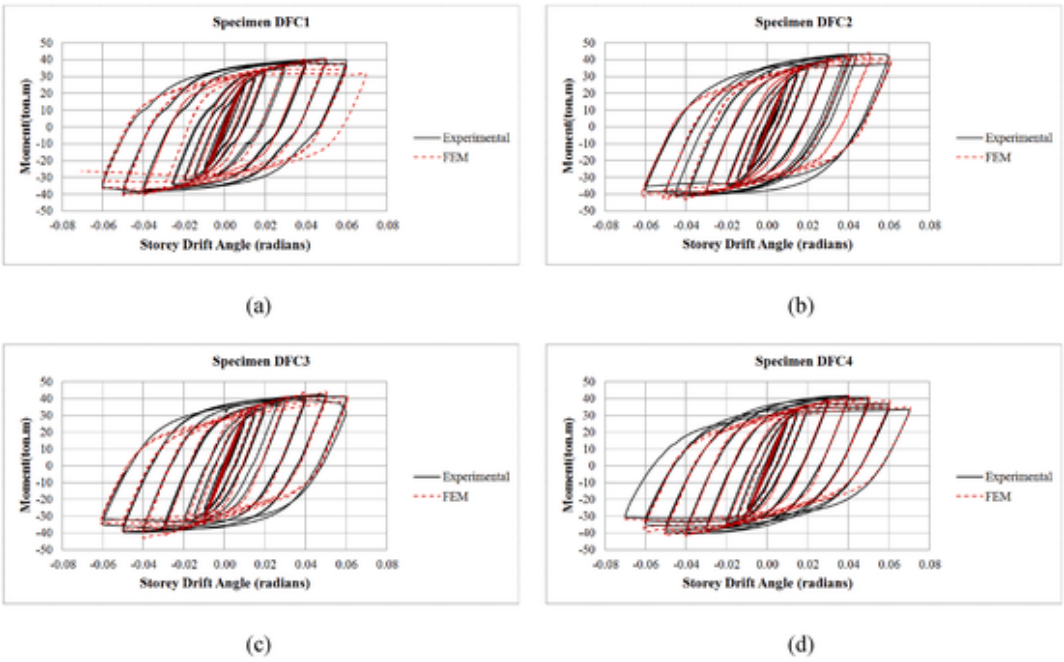

Fig. 20. Comparison of hysteretic behavior of analytical and experimental specimensa) DFC1, b) DFC2, c) DFC3, and d) DFC4.

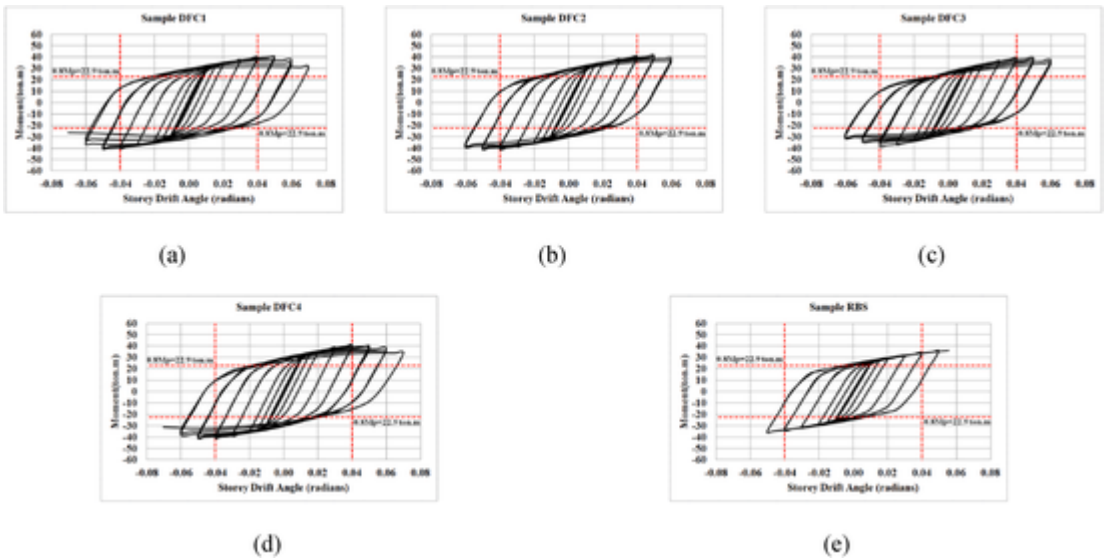

Fig. 21. Moment-rotation responses of the DFC samples besides RBS connectiona) DFC1, b) DFC2, c) DFC3, d) DFC4 and e) RBS.

flange. As a result, this grown plastic area in the beam flange increases energy dissipation and reduces the plastic strain in the groove welds.

Also, four drilling arrangements were selected to study the drilled flange connections in the frame with I-shape columns. The proposed perforated arrangement was combined DP with notches and holes (DFC1-IC), radial DP (DFC2-IC), semi radial DP with notches (DFC3-IC), and semi radial DP (DFC4-IC) drilling arrangement. Also, a reduced beam section with radius cut connection (RBS-IC) was modeled to compare the behavior of the proposed perforated beam flange connection with a conventional RBS connection. In this connection, the values of the parameters “a", “b", and “c" were considered 110, 210, and 33 mm, respectively. The maximum amount of cross-section reduction was considered 30%. The minimum plastic section modulus of the beam is 840.6 cm^3 in the reduced part. The location and diameter of the holes on the beam flange were selected, similar to the specimens with the box column. In all models, the column's height was 3090 mm, the depth of the column and beam was 300 mm, the width of the column flange was 300 mm, and the width of the beam flange was 220 mm. The thickness of the column flange and beam flange was 15 mm. The thickness of the column web was 30 mm, and the thickness of the beam web was 10 mm. Fig. 22 shows the distribution of the plastic strain of the beam

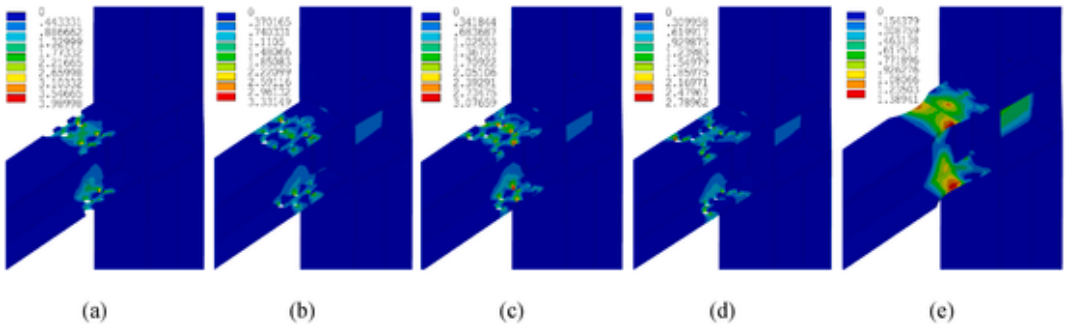

Fig. 22. Distribution of the plastic strain in the plastic hinge zone of samples in the inter-story drift angle of 0.06 radians for DFCs and 0.049 radians for RBS-ICa) DFC1-IC, b) DFC2-IC, c) DFC3-IC, d) DFC4-IC and e) RBS-IC.

at the inter-story drift angle of 0.06 radians in the proposed DFCs with the I-section columns and 0.049 radians (failure rotation) in RBS-IC connection. Due to the proper arrangements of holes and distribution of plastic strain in the plastic hinge of the beam, these connections with I-section columns are also capable of preventing the rupture of the CJP groove welds until the plastic rotation is up to 0.06 radians.

The maximum moment capacity of the analytical samples DFC1-IC, DFC2-IC, DFC3-IC, DFC4-IC, and RBS-IC is 375.3 kN.m, 395.1 kN.m, 363.8 kN.m, 382.4 kN.m, 342.2 kN.m respectively (See Fig. 23), which is 9.7%, 15.5%, 6.3%, and 11.7% higher than the RBS-IC sample. The value of plastic rotation in the samples DFC1-IC, DFC2-IC, and DFC3-IC is 0.06 radians, and the value of plastic rotation in the sample DFC4-IC is 0.07 radians. The value of plastic rotation in the sample RBS-IC is 0.049 radians.

The use of the proposed drilling arrangements of beam flange in the beam-to-column connections with the I-section column will also meet the requirements for the special moment-resisting frames.

3.4. Failure modes

The possibility of local buckling in the beam flange at a distance between the holes in the reduced area is minimized with adjusted holes spacing. Thus, the flange section is more resistant to local buckling compared to conventional RBS connections (See Fig. 19). In addition, the more stable behavior of the plastic hinge zone leads to acceptable performance in the maximum plastic rotation of 0.06 rad.

No out-of-plane buckling happened in DFC1 before 0.04 rad rotation. The first evidence of such a local buckling with 2.5 cm in length was observed along the plastic hinge at the inter-story drift angle of 0.06 rad. The rupture was initiated from the edge of the internal holes and was expanded to the beam web. The distance of the fractured section from the nearest column flange was 25.2 cm. In DFC2, the beam flange local buckling did not occur before the plastic rotation of 0.04 rad. At the inter-story drift angle of 0.06 radians, the out-of-plane buckling of the flange was observed in the 3.7 cm of plastic hinge. The flange rupture was initiated from the side holes' external edge and partially penetrated the column web. The distance of the ruptured section from the nearest column flange was 21.2 cm. In DFC3, the beam flange local buckling did not happen prior to the plastic rotation of 0.04 rad. The first evidence of the

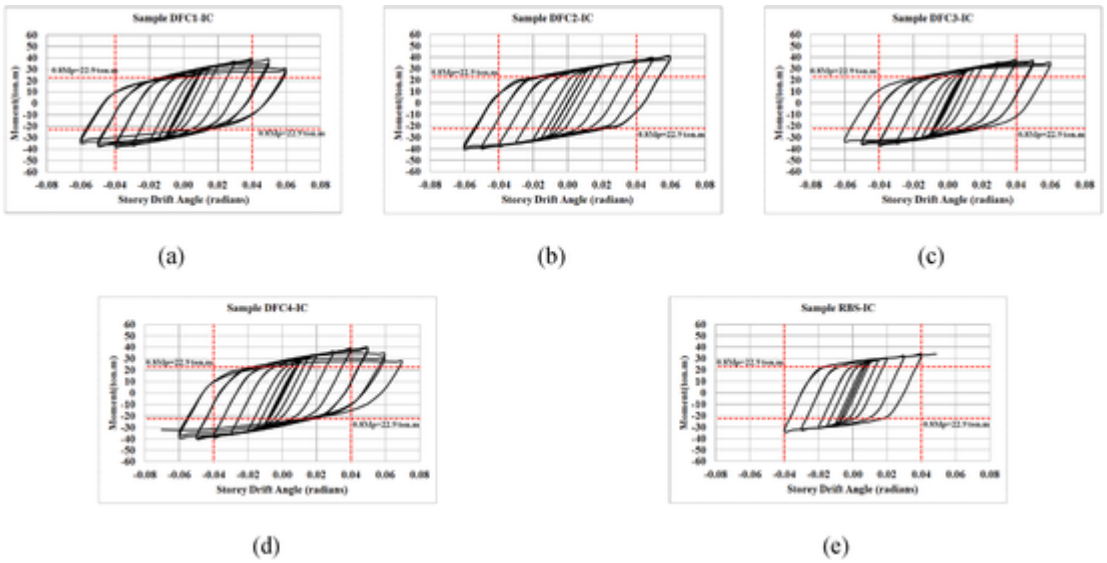

Fig. 23. Moment-rotation responses of the DFC samples with I-section column a) DFC1-IC, b) DFC2-IC, c) DFC3-IC, d) DFC4-IC and e) RBS-IC.

local buckling in DFC3 was observed at the inter-story drift angle of 0.06 rad. The measure of beam flange local buckling in the plastic hinge length was 1.8 cm. The rupture was initiated from the side of the internal hole and was partially expanded to the beam web. The distance of the ruptured section to the nearest column face was 17.3 cm. The beam flange local buckling of DFC4 was initiated at the inter-story drift angle of 0.045 rad. The measure of beam flange local buckling in the plastic hinge length was 1.3 cm. At the inter-story drift angle of 0.05 rad, the length of the buckled portion of the plastic hinge reached 1.9 cm. At the inter-story drift angle of 0.06 rad, the local lateral buckling of the beam flange increased to 3.1 cm in the plastic hinge range. At the inter-story drift angle of 0.07 rad, the length of the buckled portion increased to 4.2 cm without any rupture. Fig. 24 presents the failure modes of all specimens.

3.5. Behavior of panel zone

Fig. 25 indicates the shear strain of panel zones in the proposed DFCs. Because of the little rotation of panel zones, they behaved linearly, and thus the majority of energy dissipations took place in plastic hinges. In other words, in this type of connection, the panel zone does not play a notable role in the nonlinear behavior of the steel frame. The shear rotation of panel zones was 0.0014, 0.0021, 0.0022 and 0.0011 radians were measured in DFC1, DFC2, DFC3, and DFC4 respectively. Such results seem to indicate that the proposed DFCs were capable of transferring the inelastic portions to ductile areas of beams and prevent the column and panel zone and welds from failure.

4. Behavior of DFCs with various beam depths

The various parameters such as height and width of beams and columns, length of the beams and columns, the thickness of the plate in the construction of the beams and columns, strength of the materials, dimensions of the protected zone in the beam flange, and distance from the start of the reduce section of beam flange from the column face are effective on the flexural strength, ductility and cyclic behavior of beam-to-column connections. Also, due to the practical conditions and need for beams with different heights and lengths, it was necessary to investigate the behavior of a sample pattern (e.g., semi-radial) in various beam depths. Finite element modeling is used to investigate the effect of beam depth on the seismic behavior of DFC connections. For this purpose, analytical samples SRDFC1, SRDFC2, and SRDFC3 were designed and modeled. Geometric characteristics of experimental specimens used by Engelhardt [40] Chen and Chao [41] were considered to model SRDFC2 and SRDFC3 samples. According to ANSI/AISC358-16 [34], in RBS connections, in special moment resistance frames (SMRF), the beam's clear span-to-depth ratio is limited to 7 or greater. Also, in SMRF, the beams and columns should have seismic compact sections. In the SRDFC1 model, the column's height was 3090 mm, the depth of the beam was 300 mm, and the width of the beam flange was 220 mm. In SRDFC2 and SRDFC3, the column heights were considered 3600 mm, the length of the beams was considered 600 mm and 900 mm, respectively, and the width of the beam flange was 300 mm. Tables 7 and 8 show the dimensions of geometric characteristics of the beams and columns.

According to the beam cross-section geometry of specimen SRDFC1, the nearest hole's distance to column face “a" and the length of the reduced section “b" were 110 and 210 mm, respectively. In the analytical sample SRDFC2, the values “a" and “b" were 150 and 420 mm, respectively. In the analytical sample SRDFC3, the values “a" and “b" were 150 and 630 mm, respectively. The length values of “a" and “b" are presented in Fig. 26.

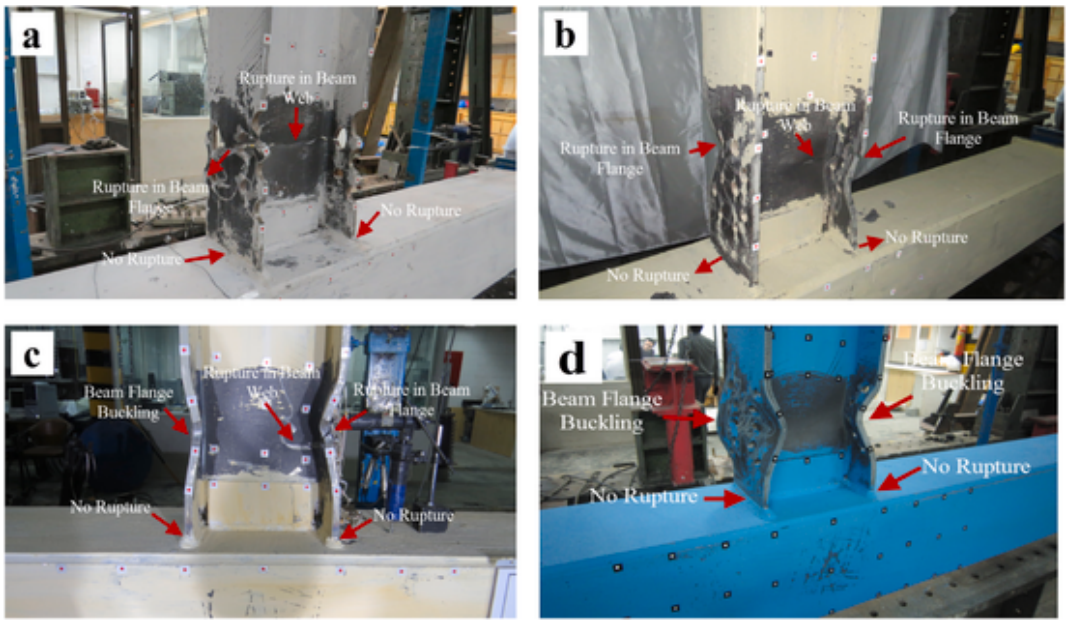

Fig. 24. Failure modes of a) DFC1, b) DFC2, c) DFC3, and d) DFC4.

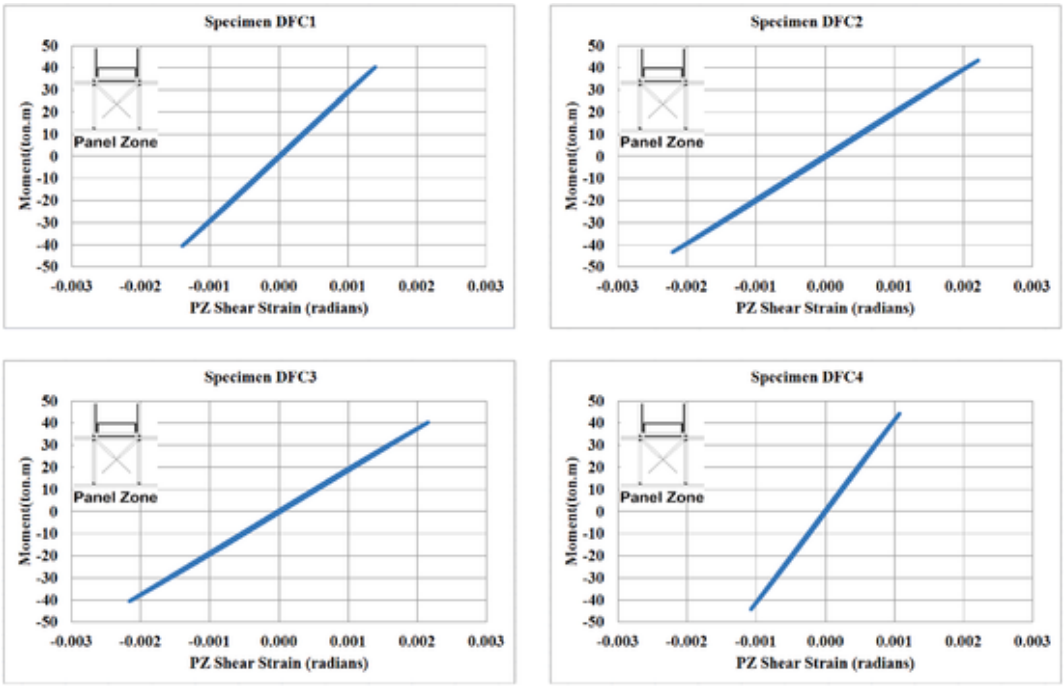

Fig. 25. The moment-shear strain curves for DFCs.

Table 7
Geometric properties of models.

Samples	Width of beam flange b_{bf} (mm)	Depth of beam d_b (mm)	Width of columns flange b_{cf} (mm)	Width of column web b_{cw} (mm)	Column height H_c (mm)	The dimension of end plate (mm)
SRDFC1	220	300	300	300	3090	350
SRDFC2	300	600	400	400	3600	450
SRDFC3	300	900	500	500	3600	550

Dimensions are in millimeters.

Table 8
Thickness of the members in selected models.

Samples	Thickness of beam flange t_{bf} (mm)	Thickness of beam web t_{bw} (mm)	Thickness of column flange t_{cf} (mm)	Thickness of column web t_{cw} (mm)	Thickness of shear tab t_{st} (mm)	Thickness of continuity plate t_{cp} (mm)	Thickness of end plate t_{ep} (mm)
SRDFC1	15	10	15	15	10	15	30
SRDFC2	20	15	25	25	15	20	30
SRDFC3	25	15	30	30	15	25	30

Dimensions are in millimeters.

In the semi radial DP of the beam flange, the analytical sample of SRDFC1 (semi radial drilled flange connection), the beam flanges were reduced in five rows (See Fig. 27), with the reductions equal to 22%, 25%, 27%, 29%, and 31. In the SRDFC2 and SRDFC3 analytical samples, the beam flanges were reduced in five rows (See Fig. 27), with the reductions equal to 20%, 25%, 30%, 35%, and 40% (See Tables 9 and 10).

Also, three RBS connections, RBS1, RBS2, and RBS3, were modeled for comparison with the proposed DFCs. For this purpose, RBS analytical samples were designed and modeled in the way that the same size RBS and DFC samples have almost similar flexural strength. In RBS1, RBS2, and RBS3 samples, the horizontal distance from the face of the column flange to the start of the radius cut, "a" are 110, 150, and 150 mm, respectively. The length of radius-cut, "b" for RBS1, RBS2, and RBS3 are 210, 420, and 630 mm, respectively. The cut length at the center of the reduced beam section, "c" for RBS1, RBS2, and RBS3, was considered 30.8, 49.5, and 51 mm, respectively. The equivalent plastic section modulus for the beam in the proposed connections SRDFC1 to SRDFC3 are 861 cm^3, 3520 cm^3, and 7094 cm^3, respectively. The value of the plastic section modulus for samples RBS1, RBS2, and RBS3 are 859.7 cm^3, 3507.6 cm^3, and 7040.8 cm^3, respectively, in the reduced area based on the maximum cross-section reduction equal to 28%, 33%, 34%, respectively. The difference between the bending capacity of the proposed DFC samples, SRDFC1, SRDFC2, and

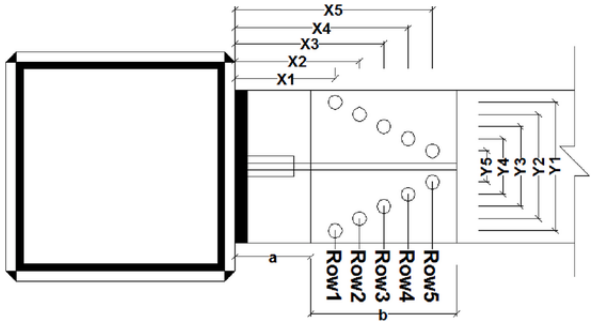

Fig. 26. Schematic holes locations in the beam flange of numerical models.

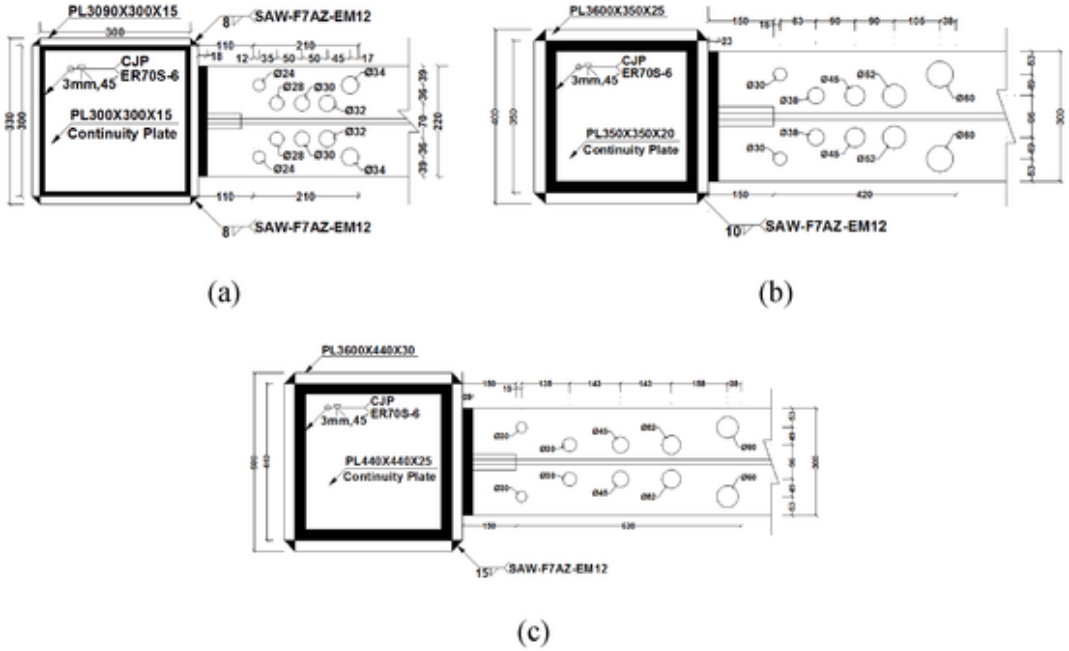

Fig. 27. Fabricating details for a) SRDFC1, b) SRDFC2, and c) SRDFC3.

Table 9
Diameter of the holes in drilling patterns of numerical models.

Analytical Samples	Pattern	Row 1 Diameter	Row 2 Diameter	Row 3 Diameter	Row 4 Diameter	Row 5 Diameter
SRDFC1		24 (22%)	28 (25%)	30 (27%)	32 (29%)	34 (31%)
SRDFC2	Semi Radial DP	30 (20%)	38 (25%)	45 (30%)	52 (35%)	60 (40%)
SRDFC3		30 (20%)	38 (25%)	45 (30%)	52 (35%)	60 (40%)

The diameter of the hole is in millimeters.

Table 10
Location of the holes in drilling patterns of numerical models.

Analytical Samples	X1	X2	X2	X2	X5	Y1	Y2	Y2	Y2	Y5
SRDFC1	122	157	207	257	303	142	70	70	70	142
SRDFC2	165	248	338	428	533	194	96	96	96	194
SRDFC3	165	300	443	586	744	194	96	96	96	194

Dimensions are in millimeters.

SRDFC3 with RBS samples RBS1, RBS2, and RBS3 is less than 0.15%, 0.35%, 0.75%, respectively. The critical locations on the CJP groove weld lines of the connections were the corner (point A) and the center (point B) of weld lines (See Fig. 28).

4.1. The cyclic behavior of analytical samples

According to the study of the analytical samples' cyclic behavior, it is observed that the SRDFC1, SRDFC2, and SRDFC3 can transmit plastic rotation 0.07, 0.07, and 0.06 radians, respectively. Also, the ratio of the maximum bending capacity of the beam to 80% of the beam's nominal flexural strength in SRDFC1, SRDFC2, and SRDFC3 samples was 1.82, 1.60, and 1.59, respectively. Also, the beam's highest strength degradation occurred in the SRDFC3 model (See Table 11). The RBS1, RBS2, and RBS3 samples can transmit plastic rotation 0.053, 0.051, and 0.048 radians, respectively. The ratio of the maximum bending capacity of the beam to 80% of the beam's nominal flexural strength in RBS1, RBS2, and RBS3 samples was 1.58, 1.37, and 1.34, respectively. Figs. 29 and 30 illustrate the hysteresis behavior curves of the analytical samples. It could be considered that the beam depth did not significantly affect the ro-

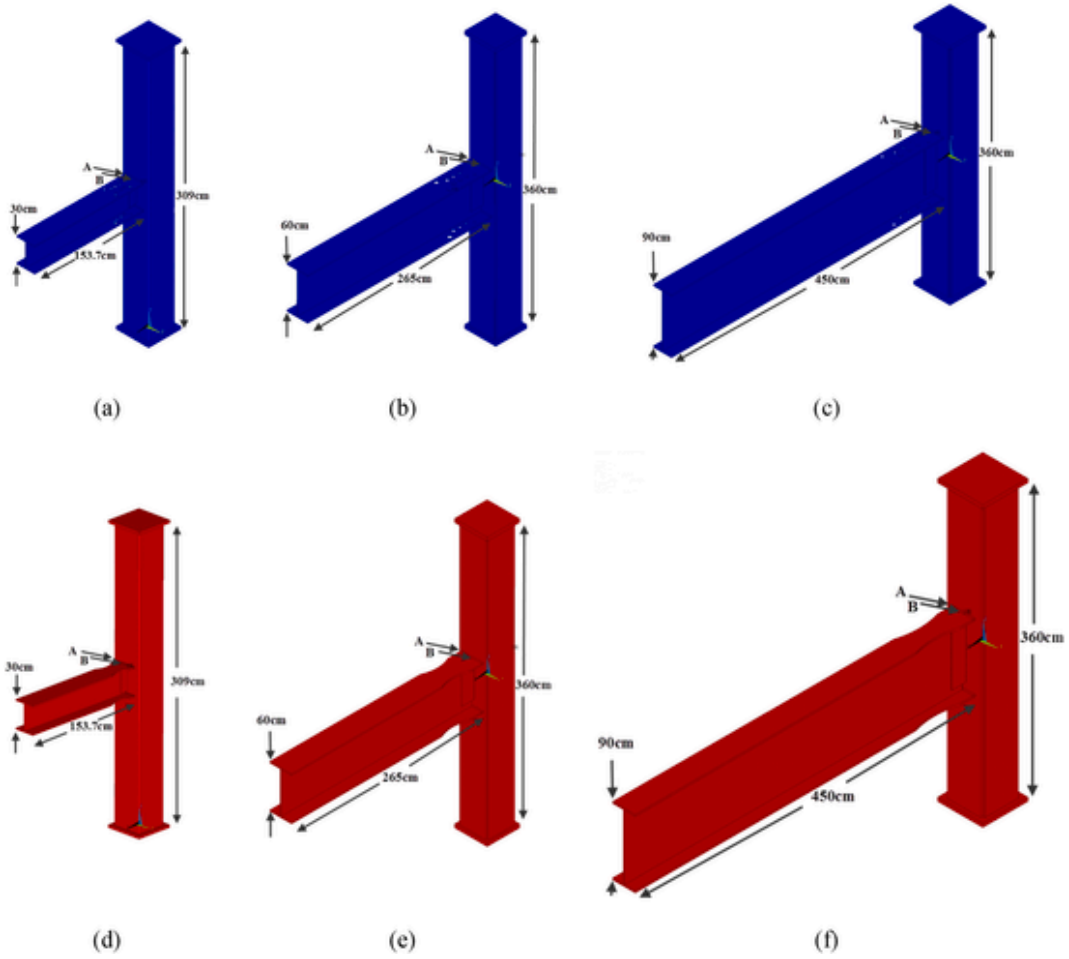

Fig. 28. FE models of a) SRDFC1, b) SRDFC2, c) SRDFC3, d) RBS1, e) RBS2 and f) RBS3.

Table 11
Summary of the analytical results corresponding to bending capacity.

Samples	θ_{pmax} (radian)	θ_y (radian)	M_y (KN.m)	M_p (KN.m)	$0.8M_p$ (KN.m)	$M_{0.04}$ (KN.m)	M_{umax} (KN.m)	M_{umin} (KN.m)	Initial Stiffness $K_{initial}$ (KN/m)	Absorbed Energy E_D (KN.m)	Maximum strength degradation of beam (%)	$M_{umax}/0.8M_p$
SRDFC1	0.07	0.00936	251.0	282.0	225.6	409.9	409.9	329.5	26820	422.3	19.6	1.82
SRDFC2	0.07	0.00833	703.9	1181.5	945.2	1383.6	1508.2	1261.1	84499	1251.4	16.4	1.60
SRDFC3	0.06	0.00883	1587.6	2363.3	1890.6	2786.9	2998.7	2269.1	179795	2133.1	24.3	1.59
RBS1	0.053	0.00931	244.7	282.0	225.6	332.7	356.5	349.5	26284	235.1	2.0	1.58
RBS2	0.051	0.00852	989.8	1181.5	945.2	1207.9	1298.3	1100.2	116174	743.5	15.3	1.37
RBS3	0.048	0.00881	1549.1	2363.3	1890.6	2526.2	2526.2	1841.3	175834	944.3	27.1	1.34

Unit: KN and m.

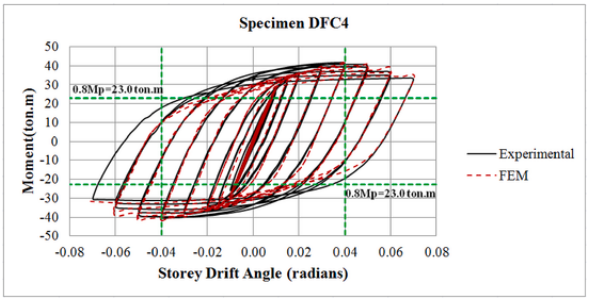

Fig. 29. Experimental and numerical Moment-rotation responses of DFC4 specimen.

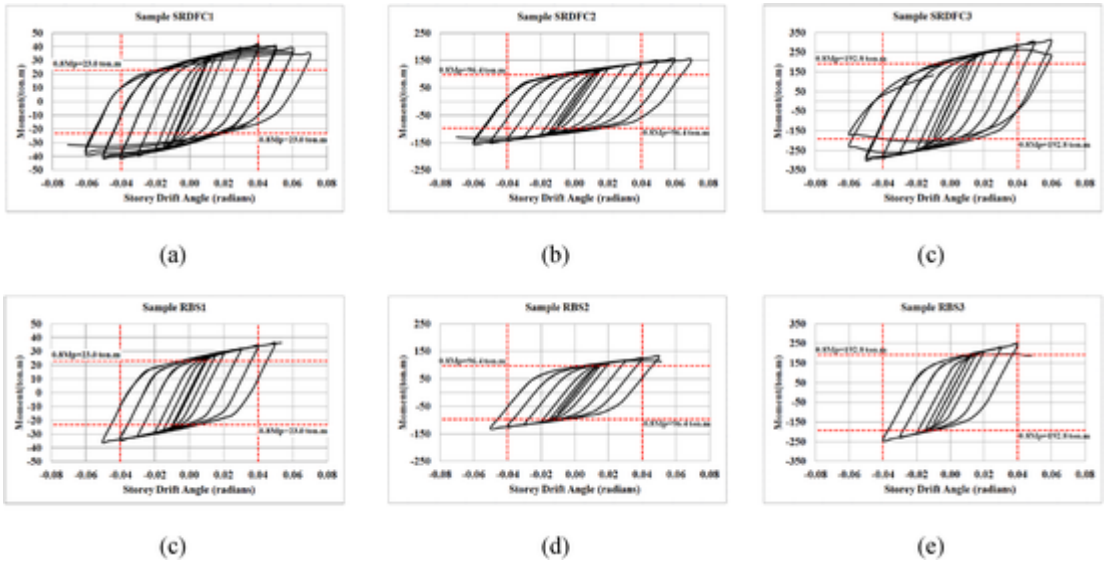

Fig. 30. Moment-rotation responses of a) SRDFC1, b) SRDFC2, c) SRDFC3, d) RBS1, e) RBS2 and f) RBS3.

tational capacity of DFCs. DFCs with the semi radial drilled pattern provide a drift angle capacity of more than 0.06 radians in all samples with different beam depths.

4.2. Distribution of damage indexes in analytical samples

For assessing the performance of analytical specimens, three important damage indexes were used. Equivalent plastic strain (EPEQ), triaxiality index (TI), and rupture index (RI) have been considered. These parameters were proposed by EL-Tawil et al. [42]. The damage indexes were used to investigate the potential for failure and rupture in the CJP groove welds and steel elements of connections. The equivalent plastic strain (EPEQ) defined as follows:

$$EPEQ = \varepsilon_{eqv}^{pl} = \sqrt{\frac{2}{3}\varepsilon_{ij}^{pl}\varepsilon_{ji}^{pl}} \tag{6}$$

where ε_{ij}^{pl} and ε_{ji}^{pl} are components of plastic strain. The EPEQI index is used to quantify the local ductility and defined as follows:

$$EPEQI = \frac{\varepsilon_{eqv}^{pl}}{\varepsilon_{y}} \tag{7}$$

The triaxiality index is the fraction of hydrostatic to Von-Mises stress and can be calculated using the following equation:

$$TI = \frac{\sigma_m}{\sigma_{eff}} \tag{8}$$

where σ_m is the hydrostatic stress, and σ_{eff} is the Von Mises stress.

This parameter is used to describe weld and steel ductile failure mode. When $-1.5 < TI < -0.75$ the failure strain reduces. If triaxiality ratios get smaller than −1.5, brittle failure may happen. When the TI has positive values, the failure strain in metallic material

reduces. The rupture index is considered as the analytical criteria for the potential of failure in metallic materials. It can be calculated as follow:

$$RI = \frac{EPEQI}{\exp(1.5TI)} \tag{9}$$

The EPEQ parameter distribution in analytical samples corresponding to 0.04 radians and 0.07 radians (ultimate rotation) was presented in Fig. 31. Also, the distribution of EPEQ parameters in the CJP groove welds was presented in Fig. 32. According to Figs. 31 and 32, increasing the beam depth increases the equivalent plastic strain on the center and corner in the CJP groove welds of the beam flange to column connection. Increasing the beam's depth caused critical EPEQ values to be shifted from reduced area to the CJP groove welds. Fig. 33 shows the triaxiality ratio and the rupture index of specimens in the CJP groove welds. The triaxiality ratio increases with the increasing depth of the beam. Also, the rupture index on the center and corner of the CJP groove weld line of the beam-to-column connection decreases with the increasing depth of the beam (See Fig. 33). The results show that these DPs could overcome issues in DFCs such as stress concentration and tearing in the reduced flange and groove welds, even in connections with more considerable beam depth. However, by increasing beam depth, the condition of the CJP groove welds is getting worse.

5. Design recommendations for suggested DPs

For detailing suggested DPs in this study, the following limits should be considered. Based on the design regulations for special moment resisting frames, the beam's plastic moment at the inter-story drift angle of 0.04 radians should be more than 80% of the beam section's nominal flexural strength (Mp). For this purpose, slenderness ratios of the beam section are proposed as follows:

$$5 \le \frac{2L_b}{d_b} \le 15 \tag{10}$$

$$20 \le \frac{d_b}{t_{bw}} \le 60 \tag{11}$$

$$6 \le \frac{b_{bf}}{2t_{bf}} \le 7.5 \tag{12}$$

In these relationships, L_b, d_b, b_{bf}, t_{bf} and t_{bw} are the length of the cantilever beam, the depth of the beam section, the width of the beam flange, the thickness of the beam flange, and the thickness of the beam web, respectively.

To achieve the ratio of the resisting moment to the nominal flexural strength greater than 1.3 for the reduced section, the percentage reduction (P.R) of the section should be in the range of 18%–50%. The P.R of the section can be calculated using the following equation:

$$P.R = (\frac{x-a}{3.125b} + 0.18) \times 100 \tag{13}$$

In the above equation, “x" is the distance from the center of the drilled holes to the face of the column, “a" is the distance from the face of the column to the edge of the nearest holes, and “b" is the length of the reduced section.

The holes' appropriate distance, location, and diameters should be followed to minimize the strain concentration between the drilled holes and prevent the rupture in a beam flange. Fig. 34 shows the configuration and distance of the holes in the proposed DPs. The appropriate locations, distances, and diameters of the holes in the beam flange can be calculated using the equations presented in Table 12.

The following proposed equations can be used to determine the probable maximum moment at the plastic hinge and the distance from the face of the column to the plastic hinge for drilled flange connections the parameters related to the position and diameter of the holes and beam cross-section. Fig. 35 shows the parameters of the position and hole diameters in the proposed DPs.

The plastic section modulus of beam flange (Z_{bxf}), plastic section modulus of beam web (Z_{bxw}), and the plastic section modulus about the x-axis of the gross section of the beam at the location of the plastic hinge (Z_{bx}) can be calculated, respectively, using the following equations:

$$Z_{bxf} = b_{bf}t_{bf}(d_b - t_{bf}) \tag{14}$$

$$Z_{bxw} = 0.25(d_b - 2t_{bf})^2 \tag{15}$$

$$Z_{bx} = Z_{bxf} + Z_{bxw} \tag{16}$$

where d_b, b_{bf}, t_{bf} and t_{bw} are the depth of the beam section, the width of the beam flange, the thickness of the beam flange, and the thickness of the beam web, respectively. Also, the plastic section modulus about the x-axis of the gross section of the beam drilled flange at the location of the plastic hinge (Z_{DFC}) calculated as follows:

$$Z_{DFC} = Z_{bx} - 2Dt_{bf}(d_b - t_{bf}) = b_{bf}t_{bf}(d_b - t_{bf}) + 0.25(d_b - 2t_{bf})^2 - 2Dt_{bf}(d_b - t_{bf}) \tag{17}$$

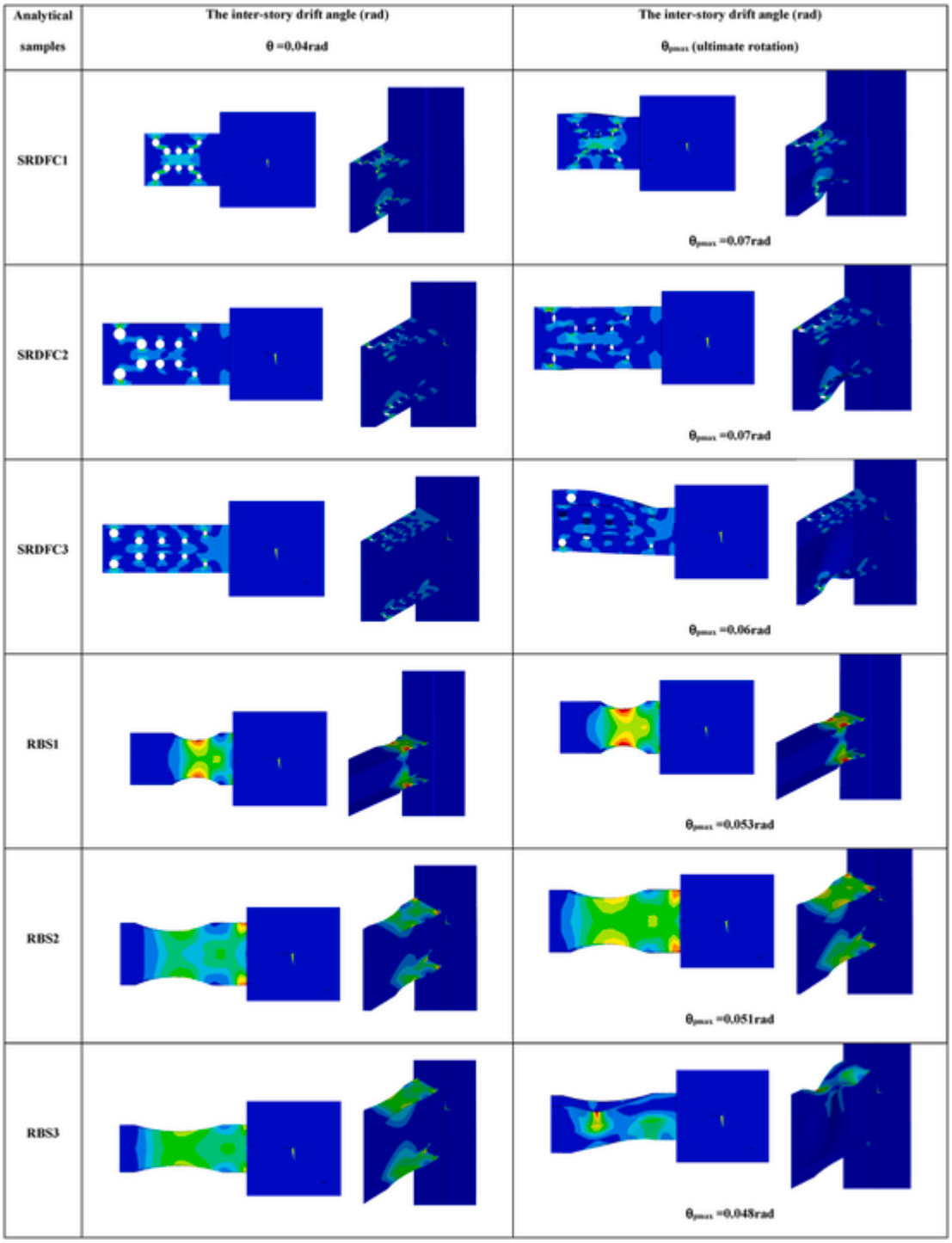

Fig. 31. Distribution of the EPEQ in semi radial drilling patterns in plastic hinge zones (The inter-story drift angle is 0.04 radians and ultimate rotation).

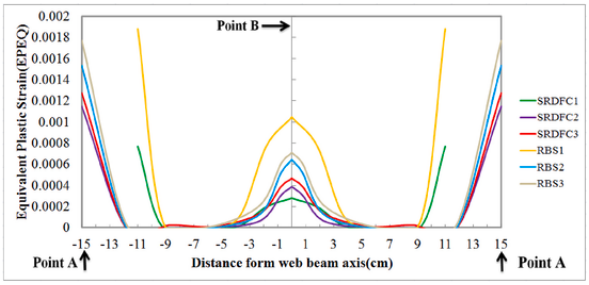

Fig. 32. Distribution of the EPEQ of analytical models in the CJP groove weld lines The inter-story drift angle is 0.04 radians).

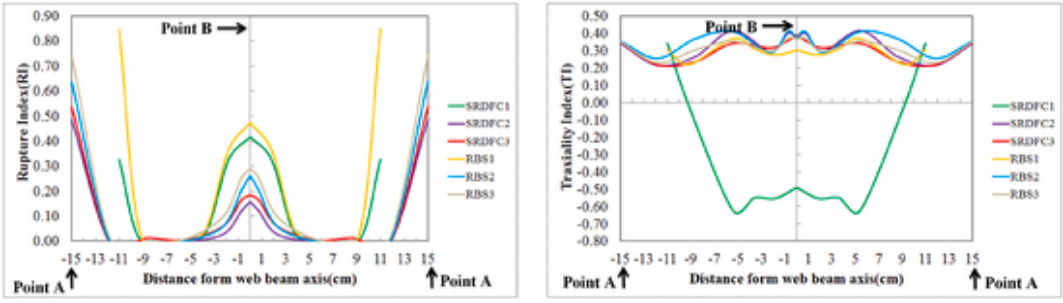

Fig. 33. Distribution of the rupture index and the triaxiality ratio of analytical models in the CJP groove weld lines (The inter-story drift angle is 0.04 radians).

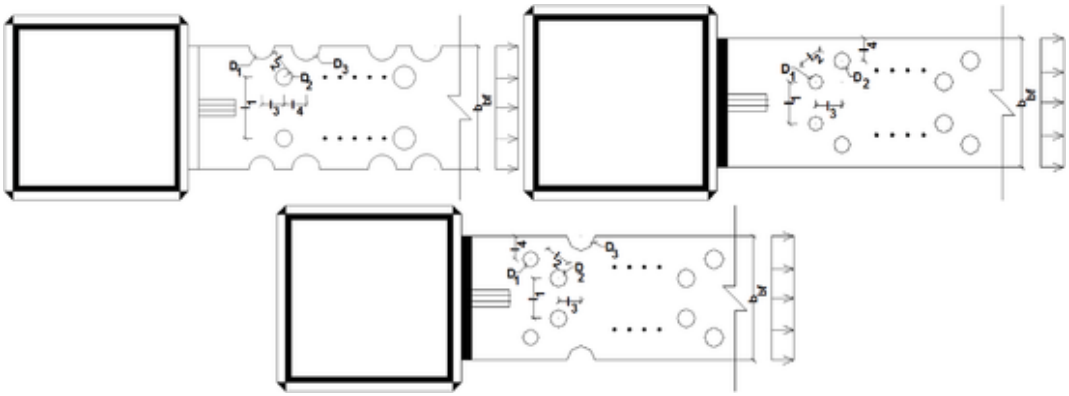

Fig. 34. Location of the beam flange holes in different configurations of DPs.

Table 12
Suggested limitations for the location, distances, and diameters of the holes in DFCs.

Drilled Pattern		
combined with notches and holes	radial	semi radial with notches and semi radial
$0.25 \leq \frac{l_1}{b_{bf}} \leq 0.65$	$0.25 \leq \frac{l_1}{b_{bf}} \leq 0.65$	$0.25 \leq \frac{l_1}{b_{bf}} \leq 0.65$
$\frac{D_2}{l_2} \geq 0.4$	$\frac{D_1}{l_2} \geq 0.4$	$\frac{D_1}{l_2} \geq 0.4$
$\frac{D_2}{l_3} \geq 0.3$	$\frac{D_2}{l_3} \geq 0.3$	$\frac{D_3}{l_3} \geq 0.3$
$\frac{D_2}{l_4} \geq 0.3$	$\frac{D_2}{l_4} \geq 0.5$	$\frac{D_1}{l_4} \geq 0.5$
$0.18b_{bf} \leq D_1 \leq 0.5b_{bf}$	$0.09b_{bf} \leq D_1 \leq 0.25b_{bf}$	$0.09b_{bf} \leq D_1 \leq 0.25b_{bf}$
$0.09b_{bf} \leq D_2 \leq 0.25b_{bf}$	$0.09b_{bf} \leq D_2 \leq 0.25b_{bf}$	$0.18b_{bf} \leq D_3 \leq 0.5b_{bf}$

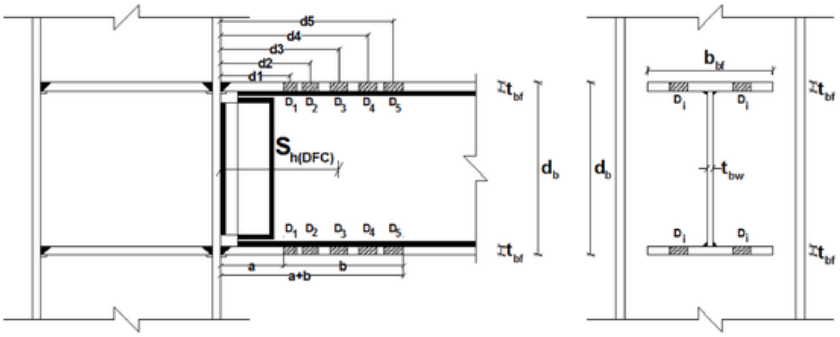

Fig. 35. Parameters of the position and hole diameters.

where D is diameter of the hole. Using the following proposed equations obtained the equivalent plastic section modulus for the beam with drilled flange ($Z_{equ(DFC)}$), the probable maximum moment at the plastic hinge ($M_{pr(DFC)}$) and the distance from the face of the column to the plastic hinge ($S_{h(DFC)}$) for drilled flange connections.

$$Z_{equ(DFC)} = \frac{\sum_i^5 d_i Z_{DFC_i}}{\sum_i^5 d_i} \tag{18}$$

$$M_{pr(DFC)} = C_{pr} R_y Z_{equ(DFC)} F_{yb} \tag{19}$$

$$S_{h(DFC)} = \frac{\sum_i^5 d_i Z_{DFC_i}}{\sum_i^5 Z_{DFC_i}} \tag{20}$$

where d_i, Z_{DFC_i}, C_{pr}, R_y, and F_{yb} are the distance of the hole from the face of the column, the plastic section modulus for drilled flange at the location of the holes, factor to account for peak connection strength, the ratio of expected yield stress to specified minimum yield stress, and yield stress for beam, respectively. Table 13 presents the proposed equivalent plastic section modulus for the beam with drilled flange, the probable maximum moment at the plastic hinge, the distance from the face of the column to plastic hinge from the proposed equation, the distance from the face of the column to plastic hinge from the experimental specimen, the bending moment corresponding to the plastic rotation of 0.04 radians, the ultimate flexural strength of the beam, the minimum plastic bending moment of beam following the local buckling of the flange, and the maximum and minimum error between the proposed moment at the plastic hinge and experimental data corresponding to bending capacity. The critical point for achieving proper performance in drilled flange connections is that the plastic strain distribution must be widespread and uniformly in the plastic hinge zone. The maximum moment of the beam occurs in the beam-column connection under lateral load in moment-resisting frames. The amount of the beam moment decreases by moving away from the column face. To have a uniform and widespread plastic strain distribution in the reduced section, the diameter of the holes should be bigger at points of the beam where the bending moments are less. Therefore, the diameter of the holes increases by moving away from the column face.

Where $S_{h(exp)}$ is the distance from the face of the column to the plastic hinge in the experimental specimens. As can be seen, the minimum and maximum error between the results of the bending capacity from proposed relationships and experimental is −0.7% and 19.53%.

In addition, it is possible to determine the diameter of the holes, the distance of the holes from the column face and each other, the probable maximum moment at the plastic hinge, and the distance from the place of the plastic hinge to the column face by presenting the proposed design relationships. The seismic behavior of these proposed connections has been investigated by using the proposed design relationships and numerical modeling of samples with different heights and spans. The proper seismic performance, reduction of equivalent plastic strain, rupture index, and prevention of stress concentration in the CJP groove welds of the beam flange to column connection can be achieved by providing the proposed design solutions.

To design the proposed drilled flange connections, first, the values of “a" and “b" can be calculated according to AISC code 358-16 [34] and relations 1 to 3. Then, to achieve the ratio of the resisting moment to the nominal flexural strength greater than 1.3 for the

Table 13
The summary of the proposed equations and experimental data corresponding to bending capacity.

Specimen	$Z_{equ(DFC)}$ (cm^3)	$M_{pr(DFC)}$ (KN.m)	$S_{h(DFC)}$ (mm)	$S_{h(exp)}$ (mm)	$M_{0.04}$ (KN.m)	M_{umax} (KN.m)	M_{umin} (KN.m)	$e_{0.04}$ (%)	e_{max} (%)	e_{min} (%)
DFC1	868	381.7	210	252	364.8	394.2	363.8	4.63	−3.17	4.92
DFC2	861	393.3	210	212	404.0	423.6	365.8	−2.65	−7.15	7.52
DFC3	863	385.6	213	173	388.3	410.9	322.6	−0.70	−6.16	19.53
DFC4	861	381.9	207	210	409.9	409.9	329.5	−6.83	−6.83	15.90

Unit: KN and mm.

reduced section, the amount of the percentage reduction of the beam flange can be considered in the range of 18%–50%, and equation (13) can be used. The percentage reduction of the beam flange can be calculated based on the distance of the hole from the column face. The diameter of the hole can be calculated based on the percentage reduction of the beam flange. Then, the relations of Table 12 can be used to minimize the stress concentration in the distance between the holes and the appropriate distance between the holes can be controlled according to the relations in Table 12. The equivalent plastic section modulus for the beam with drilled flange can be obtained by using the relation 14 to 18 after determining the diameter of the holes and their location and controlling their distances. Equation (19) is used to determine the probable maximum moment at the plastic hinge. It is also possible to calculate the distance from the face of the column to the plastic hinge by using equation (20). It is possible to have a uniform and widespread distribution of plastic strains in the plastic hinge zone by observing the arrangements and location of the holes.

6. Concluding remarks

Experimental investigations were conducted to improve the ductile behavior of DFCs. Four specimens with different radial drilling arrangements were fabricated and subjected to cyclic loading. The results are valid for welded I-beam connected to box-shaped and I-shaped columns, both made from low-yield steel. The results of this study revealed that:

1. By providing appropriate DPs on the beam flange in the plastic hinge zone and developing an eccentricity between the holes, the effective cross-sectional area of the beam flange among the holes can be increased. It was shown that DFC1, DFC2, and DFC3 were capable of tolerating a similar story drift angle of 0.06 radians, and DFC4 could tolerate story drift angle of 0.07 radians. Also, all experimental specimens with different patterns of drilled beam flange can tolerate story drift angle without considerable stiffness and strength degradations. The suggested drilled beam flange connections could meet the requirements of the special moment-resisting connections.
2. Among the examined specimens, the most significant rotational capacity belongs to DFC4. In DFC1, DFC2, and DFC3 specimens, the drift angle capacity of connections increased 50% of the minimum required rotation of the special moment-resisting connections and DFCs with simple parallel drilling patterns. However, in the DFC4 specimen, the semi-radial perforating pattern led to a more significant increase in rotational capacity and more stable cyclic behavior. Its ultimate rotational capacity was almost 75% more than the minimum required rotation of the special moment-resisting connections.
3. By selecting the appropriate perforating arrangement and considering the suitable drilling diameters, the local buckling in the plastic hinge zone in rotations less than 0.04 radians can be prevented. No evidence of local buckling and no considerable degradation in the strength and stiffness were observed in examined specimens at the inter-story drift angles of 0.04 radians or less.
4. In every tested specimen, the strains in the interior parts of beam-to-column groove welds in the beam longitudinal direction in the center parts of the weld were greater than those in the corner parts of the weld in the same direction. Moreover, in all specimens, the least strain occurred in the weld's central parts in the groove weld line direction. No observable fracture happened in the groove welds, and they behaved elastically during the tests.
5. The rotations of the panel zones of DFC1, DFC2, and DFC3 corresponding to the plastic rotation of 0.06 rad were 2.33%, 3.5%, and 3.67% of the total plastic rotation. The panel zone of DFC4 experienced a plastic rotation of 1.57% of the ultimate total plastic rotation. Such a behavior showed that the panel zones behaved elastically, and thus the plastic behavior was concentrated in the reduced areas of beams.
6. The beam depth increase does not significantly affect the maximum plastic rotation. The greater beam depth increases the equivalent plastic strain on the center and corner in the CJP groove weld line of the beam-to-column connection. The triaxiality ratio increases with the increasing depth of the beam. Also, the rupture index on the center and corner of the CJP groove welds decreases with the beam's increasing depth.

The proposed drilling arrangements, especially semicircular ones, can be considered connections with appropriate cyclic performance besides well-known RBS and RWS connections. The benefits of these connections could be achieved, provided that appropriate tools were present, with acceptable quality and accuracy, for material removal and fabrication based on the proposed drilling patterns. It should be noted that the effect of influencing factors such as floor RC slabs was neglected in this study. Hence, it is suggested to avoid connecting any element (whether welded or bolted) in the protected zone of connections.

Data availability statement

All data, models, or codes that support the findings of this study are available from the corresponding author upon reasonable request.

Declaration of competing interest

The authors declare that they have no known competing financial interests or personal relationships that could have appeared to influence the work reported in this paper.

References

[1] N.F.G. Youssef, D. Bonowitz, J.L. Gross, A Survey of Steel Moment Resisting Frame Buildings Affected by the 1994 Northridge Earthquake, NIST, Gaithersburg, MD, 1995, Report No. NISTIR 5625.

[2] S.W. Han, G.U. Kwon, K.H. Moon, Cyclic behavior of post-Northridge WUF-B connections, J. Constr. Steel Res. 63 (3) (2007) 365–374, https://doi.org/10.1016/j.jcsr.2006.05.003.

[3] M.L. Morrison, D. QSchweizer, T. Hassan, Seismic enhancement of welded unreinforced flange-bolted web steel moment connections, J. Constr. Steel Res. (2016 Jun), https://doi.org/10.1061/(ASCE)ST.1943-541X.0001575.

[4] S.J. Venture, Protocol for Fabrication, Inspection, Testing, and Documentation of Beam-Column Connection Tests and Other Experimental Specimens, 1997, p. 1997, . Rep, No, SAC/BD-97.

[5] Federal Emergency Management Agency, SAC Joint Venture, Interim Guidelines Advisory No.2Supplement to FEMA-267 Interim Guidelines: Evaluation, Repair, Modification and Design of Welded Steel Moment Frame Structures, 1999 Jun, Report No. SAC-99-11.

[6] Egor Paul Popov, Tzong-Shuoh Yang, shih-Po Chang, Design of steel MRF connections before and after 1994 Northridge earthquake, Eng. Struct. 20 (12) (1998) 1030–1038, https://doi.org/10.1016/S0141-0296(97)00200-9.

[7] Andrew Whittaker, Amir S.J. Gilani, Vitelmo Bertero, Evaluation of pre-Northridge steel moment-resisting frame joints, Struct. Des. Tall Build. 7 (4) (1998) 263–283, https://doi.org/10.1061/9780784479728.024.

[8] Swati Ajay Kulkarni, Gaurang Vesmawalab, Study of steel moment connection with and without reduced beam section, Case Stud. Struct. Eng. 1 (2014) 26–31, https://doi.org/10.1016/j.csse.2014.04.001.

[9] M.D. Engelhardt, A.S. Husain, Cyclic loading performance of welded flange bolted web connection, J. Struct. Eng. 119 (1993) 3537–3550, https://doi.org/10.1061/(ASCE)0733-9445(1993)119:12(3537).

[10] M.D. Engelhardt, T. Winneberger, A.J. Zekany, T.J. Potyraj, Experimental Investigation of Dogbone Moment Connections, American Institute of Steel Construction Inc, USA, 1997.

[11] M.D. Engelhardt, G. Fry, S. Johns, M. Venti, S. Holliday, Behavior and Design of Radius Cut, Reduced Beam Section Connections, SAC, California, 2000, Report no. 00/17.

[12] Chia-Ming Uang, Qi-Song, Shane Noel, John Gross, Cyclic testing of steel moment connections rehabilitated with RBS or welded haunch, J. Struct. Eng. (2000), https://doi.org/10.1061/(ASCE)0733-9445(2000)126:1(57).

[13] Sheng-Jin Chen, Y.C. Chao, Effect of composite action on seismic performance of steel moment connections with reduced beam sections, J. Constr. Steel Res. 57 (2001) 417–434, https://doi.org/10.1016/S0143-974X(00)00022-5.

[14] Scott L. Jones, Gary T. Fry, Michael D. Engelhardt, Experimental evaluation of cyclically loaded reduced beam section moment connections, J. Struct. Eng. (2002), https://doi.org/10.1061/(ASCE)0733-9445(2002)128:4(441).

[15] C.W. Roeder, Connection performance for seismic design of steel moment frames, J. Struct. Eng. 128 (4) (2002) 517–525, https://doi.org/10.1061/(ASCE)0733-9445(2002)128:4(517).

[16] Cheol-Ho Lee, Sang-Woo Jeon, Jin-Ho Kim, Chia-Ming Uang, Effects of panel zone strength and beam web connection method on seismic performance of reduced beam section steel moment connections, J. Struct. Eng. ASCE (2005), https://doi.org/10.1061/(ASCE)0733-9445(2005)131:12(1854).

[17] Chung Che Chou, Chia Ching Wu, Performance evaluation of steel reduced flange plate moment connections, Earthq. Eng. Struct. Dynam. 36 (Issue14) (2007) 2083–2097, https://doi.org/10.1002/eqe.714.

[18] D.T. Pachoumis, E.G. Galoussis, C.N. Kalfas, A.D. Christitsas, Reduced beam section moment connections subjected to cyclic loading: experimental analysis and FEM simulation, Eng. Struct. 31 (1) (2009) 216–223, https://doi.org/10.1016/j.engstruct.2008.08.007.

[19] F. Iannone, M. Latour, V. Piluso, G. Rizzano, Experimental analysis of bolted steel beam-to-column connections: component identification, J. Earthq. Eng. 15 (2) (2011) 214–244, https://doi.org/10.1080/13632461003695353.

[20] A. Moslehi Tabar, A. Deylami, Instability of beams with reduced beam section moment connections emphasizing the effect of column panel zone ductility, J. Constr. Steel Res. 61 (2005) 1475–1491, https://doi.org/10.1016/j.jcsr.2005.05.006.

[21] A. Deylami, A. Moslehi Tabar, Promotion of cyclic behavior of reduced beam section connections restraining beam web to local buckling, Thin-Walled Struct. 73 (2013) 112–120, https://doi.org/10.1016/j.tws.2013.07.013.

[22] D.W. Kim, S.C. Ball, H.B. Sim, C.M. Uang, Evaluation of sloped RBS moment connections, J. Struct. Eng. ASCE (2016), https://doi.org/10.1061/(ASCE)ST.1943-541X.0001459.

[23] Tzong-Shuoh Yang, Egor P. Popov, Experimental and Analytical Studies Steel Connections and Energy Dissipaters. National Science Foundation American Institute of Steel Construction, Earthquake Engineering Research Center College of Engineering University of California at Berkeley, 1995 Dec, Report No. UCB/EERC-95/13.

[24] H. Farrokhi, F. Danesh, S.A. Eshghi, Modified moment resisting connection for ductile steel frames (numerical and experimental investigation), J. Constr. Steel Res. 65 (10–11) (2009) 2040–2049, https://doi.org/10.1016/j.jcsr.2009.04.019.

[25] M. Vetr, A. Haddad, Study of Drilled Flange Connection in Moment Resisting Frames. Report No. 3732, International Institute of Earthquake Engineering and Seismology, Tehran, Iran, 2010.

[26] M. Vetr, M. Miri, A. Haddad, Seismic behavior of a new reduced beam section connection by drilled holes arrangement (RBS_DHA) on the beam flanges through experimental studies, in: 15th World Conference of Earthquake Engineering (15WCEE), Portugal, Lisbon, 2012.

[27] Sang Ju Lee, Sang Eul Han, Sam Young Noh, Sung-Woo Shin, Deformation capacity of reduced beam section moment connection by staggered holes, in: Proceedings of the International Conference on Sustainable Building Asia, 2007, pp. 1067–1072, Seoul, Korea. http://www.irbnet.de/daten/iconda/CIB8242.pdf.

[28] Ardavan Atashzaban, Iman Hajirasouliha, Roohollah Ahmady Jazany, Mohsen Izadinia, Optimum drilled flange moment resisting connections for seismic regions, J. Constr. Steel Res. 112 (2015) 325–338, https://doi.org/10.1016/j.jcsr.2015.05.013.

[29] Roohollah Ahmady Jazany, Improved design of drilled flange (DF) moment resisting connection for seismic regions, Bull. Earthq. Eng. (2018), https://doi.org/10.1007/s10518-017-0265-9.

[30] M. Tahamouli, H. Roudsari, K. Jamshidi, M. Torkamana, M. S.Ganji, Experimental and numerical investigations of rigid IPE beam connections with drilled flange and web stiffener, Ins. Struct. Eng. 16 (2018) 303–316, https://doi.org/10.1016/j.istruc.2018.10.008.

[31] Shadman Heidari Peyman, Armin Aziminejad, A.S. Moghadam, Mohammad Ali Jafari, Evaluation of drilled flange connections with combined arrangements of holes and notches, Bull. Earthq. Eng. (2020), https://doi.org/10.1007/s10518-020-00920-1.

[32] AISC, Specification for Structural Steel Buildings, ANSI/AISC 360–16, American Institute for Steel Construction, Chicago, 2016.

[33] AISC, Seismic Provisions for Structural Steel Buildings, ANSI/AISC 341–16, American Institute for Steel Construction, Chicago, 2016.

[34] AISC, Prequalified Connections for Special and Intermediate Steel Moment Frames for Seismic Applications, American Institute for Steel Construction, Chicago, 2016, ANSI/AISC 358-16.

[35] FEMA-355D, State of the Art Report on Connection Performance, Federal Emergency Management Agency, 2000.

[36] FEMA-360, Recommended Seismic Design Criteria for New Steel Moment-Frame Buildings, Federal Emergency Management Agency. Washington D.C., 2000.

[37] ASTM-A370-14, Standard Test Methods and Definitions for Mechanical Testing of Steel Products, 2014.

[38] ANSYS, Meshing User's Guide. Release 16.0, ANSYS Inc, 2016.

[39] A. Elkady, D. Lignos, Analytical investigation of the cyclic behavior and plastic hinge formation in deep wide-flange steel beam-columns, Bull. Earthq. Eng. 13 (4) (2015) 1097–1118, https://doi.org/10.1007/s10518-014-9640-y.

[40] M.D. Engelhardt, Design of reduced beam section moment connections, in: Proceedings, North American Steel Construction Conference, 1, 1999, Toronto Canada, pp. 1–1 to 1–29.

[41] S.J. Chen, Y.C. Chao, Effect of composite action on seismic performance of steel moment connections with reduced beam sections, J. Constr. Steel Res. 54 (2001) 417–434, https://doi.org/10.1016/j.jcsr.2005.05.006.

[42] S. El-Tawil, T. Mikesell, E. Vidarsson, S. Kunnath, Strength and Ductility of FR Welded Bolted Connections. Rep No. SAC/BD-98/01 Sacramento CA SAC Joint Venture, 1998.